Title

A new mechanism of posttranslational polyglutamylation regulates phase separation and signaling of the Wnt pathway protein Dishevelled.

Authors

Marek Kravec[1], Ondrej Šedo[2], Jana Nedvědová[3,4], Miroslav Micka[1,2], Marie Šulcová[1], Nikodém Zezula[1], Kristína Gömöryová[1], David Potěšil[2], Ranjani Sri Ganji[2], Igor Červenka[1], Zbyněk Zdráhal[2], Jakub Harnoš[1], Konstantinos Tripsianes[2], Carsten Janke[5,6], Cyril Bařinka[3] and Vítězslav Bryja[1*]

Affiliations

1. Department of Experimental Biology, Faculty of Science, Masaryk University, Brno, Czech Republic.

2. Central European Institute of Technology (CEITEC), Brno, Czech Republic.

3. Institute of Biotechnology of the Czech Academy of Sciences, BIOCEV, Prague, Czech Republic.

4. Department of Biochemistry, Faculty of Science, Charles University, Prague, Czech Republic.

5. Institut Curie, Université PSL, CNRS UMR3348, Orsay, France

6. Université Paris-Saclay, CNRS UMR3348, Orsay, France

* Corresponding author: bryja@sci.muni.cz

Abstract

Polyglutamylation is a reversible post-translational modification that is catalyzed by enzymes from the tubulin tyrosine ligase-like (TTLL) family. Here, we found that TTLL11 generates a previously unknown type of polyglutamylation initiated by the addition of a glutamate residue to the free C-terminal carboxyl group of a substrate protein. TTLL11 efficiently polyglutamylates the Wnt signaling protein Disheveled 3 (DVL3), thereby changing the interactome of DVL3, as well as it increases its capacity to get phosphorylated, to undergo liquid-liquid phase separation (LLPS), and to act in the non-canonical Wnt pathway. Both carboxyterminal polyglutamylation and the resulting reduction in LLPS capacity of DVL3 were reverted by the deglutamylating enzyme CCP6, which demonstrates the causal relationship between TTLL11-mediated polyglutamylation and LLPS. We thus discovered a novel type of posttranslational modification, which significantly broadens the range of proteins that can be modified by polyglutamylation and provides the first evidence that polyglutamylation can act as a regulator of protein LLPS.

MAIN TEXT

Introduction

Polyglutamylation is a reversible post-translational modification (PTM) initially discovered on tubulin (*1*) that is catalyzed by several members of the tubulin tyrosine ligase-like (TTLL) protein family (*2*). Humans possess 13 TTLL homologues of which 9 are active glutamylases. According to the current understanding, tubulin polyglutamylation is initiated by the formation of the branching point by the addition of glutamate onto a γ-carboxyl group of a glutamate residue within the substrate, followed by the addition of multiple glutamates thereby generating secondary glutamate chains of variable lengths. Individual TTLL polyglutamylases show catalytic preferences either for the initial branching or the elongation of glutamate chains (*3, 4*). Moreover, individual enzymes also show preferences for different substrates such as α- or β-tubulin (*3*), or other, non-tubulin proteins out of which only a few have so far been identified (*5-7*). Polyglutamylation is a reversible modification; deglutamylation is catalyzed by enzymes from the cytosolic carboxypeptidase (CCP) family (*8-10*).

In our proteomic datasets, we discovered Dishevelled (DVL), a highly conserved regulatory protein in the Wnt signaling pathway, as a candidate binding partner of several TTLLs. Wnt pathways represent evolutionary conserved signaling modules that are required for multiple processes during the development and maintenance of homeostasis. The best studied is the Wnt/β-catenin pathway (also referred to as "canonical") where DVL is necessary for membrane signalosome complex formation (*11, 12*) which triggers the disruption of cytoplasmic β-catenin destruction complex and subsequent stabilization of β-catenin. β-catenin is translocated into the nucleus where it activates T-cell factor/lymphoid enhancer factor (TCF/LEF) dependent transcription (*13*). Another important branch is the the Wnt/planar cell polarity (Wnt/PCP) pathway, which is responsible for polarized cellular orientation and cytoskeletal rearrangements during morphogenetic cell movements (*14*). DVL is an essential transducer in Wnt/PCP pathway, but the mechanistic understanding of its functions remains elusive (*15, 16*). All three human DVL paralogs – DVL1, DVL2 and DVL3 act as common components for most, if not all, Wnt signaling branches (*17-19*). DVL was proposed to act as a branching point between individual downstream signaling pathways. How this function is achieved is unclear, but it is expected that numerous DVL interacting partners and modulation of DVL function by complex PTMs, primarily phosphorylation (*20*), have a key role. In addition to the role of DVL in Wnt pathways, it was shown to be localized in the basal bodies of cilia, affecting their positioning (*21*), in the centrosome interacting with core centrosomal proteins (*21, 22*) or in the spindle poles and kinetochores during the mitosis (*23*).

DVL and its interacting partners can form cytoplasmic puncta that have all the features typical for biomolecular condensates (*24-28*). In recent studies, endogenous DVL puncta were observed asymmetrically localized to the vegetal pole of sea urchin or sea star embryos as a part of an axis-defying event (*29, 30*). In mammalian cells, endogenously tagged DVL2 formed condensates associated with centrosomal structures that were affected by cell cycle progression or Wnt signaling activity (*28*). The puncta formation, mediated by the liquid-liquid phase separation (LLPS), has been shown to be regulated by phosphorylation, especially by phosphorylation mediated by casein kinase 1 (CK1) δ and ε (*31, 32*). However, no other PTM has so far been shown to modulate the LLPS behavior of DVL.

Following our observation of interactions between DVL and TTLL enzymes, we aimed at determining whether DVL is a substrate of polyglutamylation, and whether this is of biological importance. Testing all TTLL glutamylases, we found that TTLL11 can efficiently polyglutamylate DVL3. Surprisingly, the modification takes place via the addition of a polyglutamate chain at the α-carboxyl of C-terminal methionine of DVL3, and not, as so-far described as a branched (secondary) amino acid chain to the γ-carboxy group of the internal glutamate (*33*). DVL3 polyglutamylation changed the interactome of DVL3, in cells lowered its propensity to undergo LLPS, and increased the activity in the Wnt/PCP pathway in *Xenopus* embryos. Both C-terminal polyglutamylation and its impact on LLPS were reverted by the enzymatic activity of the CCP6 deglutamylase, suggesting that DVL3 polyglutamylation is a physiologically relevant regulatory mechanism.

Results

DVL proteins are polyglutamylated by TTLL11

We have recently identified several members of the TTLL protein family in the pull-downs of DVL3 (datasets partially published in (*34*), see **Suppl. Table 1**), suggesting that TTLLs and DVL can interact. To assess whether any of the TTLLs can polyglutamylate DVL we overexpressed all 13 mouse TTLL paralogs together with Flag-tagged human DVL3 and performed western blotting (WB) analysis (**Fig. 1A, B**). We detected a change in the electrophoretic mobility of DVL3 when overexpressed with TTLL11, which indicated that TTLL11 might have modified DVL3. Moreover, analysis of polyglutamylation by an polyE antibody, which specifically recognizes C-terminal polyglutamate peptides comprising at least 3 glutamates (*9*), revealed a prominent specific band in the presence of TTLL11 (in addition to signal corresponding to tubulin that served as a positive control) at the size of DVL3 (**Fig. 1B**). This signal was even more prominent when we used human TTLL11 (hTTLL11), indicating a higher efficiency of the human ortholog. We thus decided to use hTTLL11 in all subsequent experiments (unless specified otherwise). Importantly, co-expression of DVL3 with ligase-dead hTTLL11 (E531G) did not produce any polyglutamylation signal, revealing that the modification depends on the enzymatic activity of TTLL11 (**Fig. 1C**). The same experiments were performed with DVL2 and yielded identical results (**Fig. S1A-C**). Next, we performed co-immunoprecipitation (co-IP) of DVL3 and TTLL11 (**Fig. 1D**) and could demonstrate that both proteins are not only present in one complex, but that DVL3 is also robustly polyglutamylated (**Fig. 1D**, WB: polyE). Similar results were obtained with other DVL paralogs DVL1 and DVL2 **(Fig. S1D)**. To show whether TTLL11 polyglutamylates DVL at endogenous levels, we performed IP of endogenous DVL3 and DVL2 in the presence and absence of exogenous TTLL11. As shown in **Fig. 1E**, both endogenous DVL3 and DVL2 were polyglutamylated (**Fig. 1E**). Together this demonstrates that DVL proteins are substrates of TTLL11. In the further steps, we focused on DVL3 in order to describe the molecular details and significance of DVL3 polyglutamylation.

TTLL11 polyglutamylates DVL3 at the C-terminal methionine

To map the polyglutamylation site(s) of DVL3, we first performed domain mapping using a series of truncated versions of DVL3. All three human DVL paralogs have the same domain organization with an N-terminal DIX (Dishevelled, Axin), a central PDZ (Post-synaptic Density Protein-95, Disc Large Tumor Suppressor, and Zonula Occludens-1), and

the most C-terminal DEP (Dishevelled, Egl-10, and Pleckstrin) domain. These conserved domains are connected and C-terminally extended by intrinsically disordered regions (*17*). As shown in **Fig. 2A** (for raw data see **Fig. S2A**), the DVL3 C-terminus was essential for the polyglutamylation by TTLL11 as detected by the polyE antibody (IP Flag, WB PolyE). Posttranslational polyglutamylation is generated on glutamate residues of the primary peptide chain on tubulin (*1*) and also on the non-tubulin substrates like nucleosome assembly protein (NAP) (*5*). Replacement of glutamate by the highly similar amino acid aspartate within the polyglutamylation site of tubulin completely abolished tubulin modification in *Tetrahymena*, an effect that can be explained by the structure of TTLL (*4, 35*). Since we have observed polyglutamylation of all DVL paralogs (**Fig. 1**), we mutated all glutamates (E) conserved in the C-terminus (corresponding to aa 496-716 of DVL3) of DVL1, DVL2 and DVL3 into aspartates (D). Subsequently, we compared polyglutamylation levels of wild-type (WT) and E571D/E604D/E693D/E710D DVL3 using the polyE antibody, and, strikingly, did not observe any differences (**Fig. S2B**).

To identify the exact polyglutamylation site on DVL3, we used a mass spectrometry (MS) approach schematized in **Fig 2B**. Analysis of tryptic digests of DVL3, which was co-expressed with TTLL11 in HEK293 and immunoprecipitated, by LC-MS/MS mapped polyglutamylation to the very last C-terminal DVL3 tryptic peptide – MAMGNPSEFFVDVM – with the most abundant peaks corresponding to peptides with an additional 7-9 glutamate residues (**Fig 2Ca, b**). Of note, the peptide contains three methionine residues (M703, M705, and M716) that get partially oxidized during sample processing. In Fig. 2C, we present signals for the fully oxidized peptide; for the experiment where we performed analysis of all oxidation variants, see **Fig. S2C, D**.

We hypothesized that, similarly to tubulin and NAP, glutamylation of this peptide is realized by branching and further polyglutamate chain extension at the sole internal glutamate (E710). Interestingly, however, the E710D DVL3 mutant was polyglutamylated to the same extent as DVL3 WT (**Fig. 2Cc**). Detailed analyses of peptide fragmentation by MS/MS suggested the presence of a linear chain of glutamic acid residues after C-terminal M716 of the peptide, which was visible, especially in *b*- and *y*-ion series (**Fig. 2D**). Such a modification, i.e., the elongation of the primary amino acid chain, was unexpected because it has never been reported before. Comparison of the MS/MS spectra of the C-terminal tryptic peptide of *in-cell* polyglutamylated DVL3 and synthetic peptides mimicking polyglutamylation either via branching at the internal E710 or by C-terminal elongation **(Fig. S3)** further supported this assumption. Among the MS/MS fragments of *in-cell* polyglutamylated DVL3, we did not find any fragments characteristic of branched peptide but observed several fragments unique for the linear polyglutamylated peptide (Fig. S3). Altogether, our data strongly support the notion that TTLL11 catalyzes a so-far unknown type of polyglutamylation that extends the primary peptide sequence of DVL3 by the addition of multiple glutamates beyond the C-terminal methionine residue.

In order to directly prove C-terminal polyglutamylation at M716, we immunoprecipitated DVL3 that was co-expressed with TTLL11 and performed cyanogen bromide (CNBr) cleavage of the mixture of DVL3 tryptic peptides. CNBr cleaves peptide bonds at the C-terminus of non-oxidized methionine residues, releasing peptides with C-terminal homoserine (Hse) or homoserine lactone (Hsl) (**Fig 2E**). After CNBr cleavage, the peak series corresponding to polyglutamylated MAMGNPSEFFVDVM disappeared (**Fig. 2Ea**), and instead non-glutamylated peptides terminated either by Hse or Hsl appeared (**Fig. 2Eb**). In addition, after CNBr treatment, we could detect signals corresponding to free

polyglutamate chains of 10 - 15 glutamate residues (**Fig 2Ec**). This effect was the most obvious in the double oxidized peptide (Fig. 2E), but the other oxidized forms of the C-terminal peptide showed similar results with the notable exception of the fully oxidized peptide that could not be digested by CNBr and thus conveniently served as a negative control (**Fig S4A-D)**. These results independently confirmed that DVL3 is polyglutamylated by the extension of the C-terminal M716 and provided further evidence for the existence of this novel type of PTM catalyzed by TTLL11.

Sequence determinants of TTLL11-mediated DVL3-polyglutamylation

To determine molecular signatures of C-terminal polyglutamylation catalyzed by TTLL11, we generated a panel of DVL3 C-terminal mutants, where we (1) mutated the C-terminal glutamate residue 710 to aspartate (E710D); (2) mutated both acidic residues to alanines (E710A/D714A); (3) elongated the main polypeptide chain by the addition of four glutamate (4E) or four alanine (4A) residues; and (4) generated truncated variants lacking the C-terminal tail (DVL3 1-709; 1-697) (**Fig. 3A**). These mutants were then compared for their capacity to be modified by TTLL11. To this end, DVL3 was immunoprecipitated and polyglutamylation was analyzed by WB with the polyE antibody (**Fig. 3B, C**), as well as by MS-based detection (**Fig. S5A**). Results from both experimental approaches were in good agreement (compare Fig. 3B and Fig. S5A) and pinpointed several important facts. First, the modification is not strictly dependent on the presence of M716 or the exact C-terminal sequence as such because truncation mutants DVL3 1-697 and 1-709 as well as DVL3-4A were modified similarly to DVL3. Second, DVL3 E710A/D714A was not polyglutamylated at all and as such it could serve as a negative non-glutamylatable DVL3 control in subsequent functional experiments. Third, TTLL11 was clearly much more efficient in the polyglutamylation of DVL3-4E with the preexisting glutamate chain. To further study this effect, we generated DVL3 with only one extra glutamate (DVL3-E) at its C-terminus. As shown in **Fig. S5B** already addition of one glutamate was sufficient to enhance polyglutamylation when compared to DVL3 WT.

In order to prove that TTLL11 directly polyglutamylates DVL3, we set up an *in-vitro* polyglutamylation reaction using purified recombinant full-length DVL3 and TTLL11. We used DVL3 WT, DVL3-E, and the glutamylation-defective E710A/D714A mutant. Following *in vitro* incubation, the assay mixtures were analyzed by WB (**Fig. 3D**) and MS (**Fig. 3E a-d**). Using WB, we could detect *in vitro* polyglutamylation by the polyE antibody only on DVL3-E. Interestingly, MS analysis not only confirmed polyglutamylation of DVL3-E but also detected monoglutamylated as well as polyglutamylated peptides in the DVL3 WT sample to a lower degree. This result suggests that TTLL11 itself is capable of DVL3 polyglutamylation but the ligation of the first glutamate can represent the rate-limiting step. It is possible that the *in-vitro* assay with purified components is less efficient than polyglutamylation of DVL3 in cells, which could explain the difference in a number of added glutamates between these two assays. Notwithstanding this difference, our *in-vitro* assay unambiguously demonstrates the direct and cofactor-independent modification of DVL3 by TTLL11

Polyglutamylation changes DVL3 interactome

Polyglutamylation adds a significant negative charge to target proteins and it might regulate protein-protein interactions of DVL3 as proposed for polyglutamylation of microtubules (MT) (*36*). We thus decided to analyze how the interactome of DVL3 changes

upon polyglutamylation. We overexpressed WT or glutamylation-defective (E710A/D714A) DVL3 in the presence and absence of TTLL11, performed a pull-down of DVL3, and identified interacting partners by tandem MS (MS/MS) (for schematics see **Fig. 4A**). The differences in the interactome of DVL3 and DVL3 polyglutamylated by TTLL11 are shown in the Volcano plot in **Fig. 4B**. Numerous proteins showed a change in the binding to polyglutamylated DVL3 in presence of TTLL11. To restrict these putative hits to those that are most likely caused by DVL3 polyglutamylation and not by interaction with TTLL11, we performed an additional comparison using REPRINT with integrated CRAPOME and SAINTexpress tools (**Fig. 4C**). This bioinformatic pipeline allows comparison of multiple samples and efficiently removes false positives (*37, 38*). Proteins significantly changed in REPRINT analysis are highlighted in black in Fig. 4B. We have focused on those REPRINT patterns (Fig. 4C) where TTLL11 decreased/increased abundance in the pulldown of wild type but not glutamylation defective E710A/D714A DVL3. Such polyglutamylation-dependent pattern identified several candidates whose interaction with DVL3 can be reduced (SRSF9, DAP3, GRWD1) or increased (KATNAL2, RAB11FIP5) upon DVL3 polyglutamylation. These proteins were not reported as DVL-interacting partners before (*39*), which was, however, not the case for other hits – casein kinase 1 (CK1) δ and ε (CSNK1D and CSNK1E). These enzymes are known as major kinases regulating the functions of DVL (*40*).

DVL3 polyglutamylation controls DVL3 activity in the Wnt/PCP but not Wnt/β-catenin signaling

We next aimed at determining the biological function of DVL polyglutamylation. DVL plays a key role in the activation of Wnt/β-catenin signaling, which induces T cell factor/lymphoid enhancer factor (TCF/LEF)-dependent transcription. We thus first performed a series of experiments using TCF/LEF luciferase reporter (TopFlash assay) (schematized in **Fig. S6A**). To test the impact of TTLL11 and DVL polyglutamylation on the Wnt/β-catenin signaling pathway. Interestingly, co-expression of TTLL11 with DVL1 (**Fig. S6Ba**) or with DVL3 in combination with its activating kinase CK1ε (*41*) (**Fig. S6Bb**) efficiently reduced the TopFlash signal. Importantly, the luciferase signal decreased upon co-expression of both, WT as well as catalytically inactive TTLL11 (E531G); (Fig 4SB). This suggests that the excess of TTLL11 inhibits Wnt/β-catenin signaling independently of its enzymatic activity and represents an artifact. Indeed, TTLL11 (E531G) was as potent in inhibiting the TopFlash reporter as TTLL11 WT, even under conditions that bypass the need for DVL by expressing the constitutively active mutant of the key Wnt receptor LRP6 (LRP6ΔN) (*42*) (**Fig S6Bc, d**). The mechanism of how TTLL11 inhibits Wnt/β-catenin is unclear, but this fact thwarted our efforts to determine the molecular function of DVL3 polyglutamylation by simply overexpressing TTLL11.

As an alternative approach, we studied the properties of DVL3 WT, polyglutamylation-mimicking DVL3 with 4 and 12 C-terminally added glutamates (DVL3-4E and DVL3-12E), and glutamylation defective DVL3 (E710A/D714A). First, we have tested to what extent DVL3-4E/12E and DVL3 E710A/D714A can transduce signals induced by Wnt3a. Rescue assays in *RNF43/ZNRF3/DVL1/DVL2/DVL3 penta* knockout cells (DVL PKO) (*43*) suggested that, albeit slightly less efficient than DVL3 WT, both DVL3-4E and -12E can well mediate Wnt3a-induced signaling (**Fig. S6Ca**). Non-modifiable DVL3 E710A/D714A mutant showed reduced, but still potent ability to transduce Wnt3a-induced signaling. However, this DVL3 variant was repeatedly observed at lower levels in comparison to DVL3 WT or DVL3-12E (see **Fig. S6Cb**), and as such we

do not think that the result reflects the lower capacity of DVL3 E710A/D714A to transduce Wnt-3a signal. In line with our observation that polyglutamylation does not affect the function of DVL3 in Wnt/β-catenin signaling, co-expression of DVL3-activating kinase CK1ε with both DVL3 WT and DVL3-12E potentiated TCF/LEF-dependent transcription to similar levels (**Fig. S6D**). Additionally, Wnt ligands were unable to modify DVL3 interaction with TTLL11 or TTLL11-induced polyglutamylation of DVL3 (**Fig S6E**). We thus conclude that polyglutamylated DVL3 is proficient in the Wnt/β-catenin signaling and DVL3 polyglutamylation does not directly affect DVL role in canonical Wnt pathway.

To address the possible role of DVL3 polyglutamylation in the non-canonical Wnt/PCP signaling, we have used the well-established model of the *Xenopus laevis* embryos (*44*). Wnt/PCP in the *Xenopus* model controls the process of convergent extension (CE) during gastrulation and neurulation. The role of candidate proteins in CE can be assessed by the injection of mRNA or inhibitory morpholinos (MO) (for experimental schematics and scoring system, see **Fig. 5A, B**. Injection of the *Xenopus* (x) Dvl3 mRNA affected CE but, strikingly, the polyglutamylation-mimicking variant xDvl3-12E triggered CE defects much more efficiently (**Fig. 5C**). To strengthen this observation, we have analyzed also an earlier developmental event – blastopore closure (**Fig. S7A**). The blastopore closes at stage 11.5; but gets delayed when CE movements mediated by PCP signaling are disrupted (**Fig. S7B**). In line with data in Fig. 5C, polyglutamylated xDvl3-12E was able to delay the blastopore closure to a larger extent than xDvl3 WT (**Fig. S7C**). The WB analysis in the embryo lysates confirmed that the levels of individual xDvl3 variants were comparable (**Fig. S7D**). Interestingly, *xTTLL11* expression peaks exactly when CE movement during gastrulation starts (stages 8-11) in *X. laevis* embryos (**Fig. S7E, F**). We have thus downregulated xTTLL11 by MOs targeting either its start codon (**Fig. 5D**) or splicing site (**Fig. S7G**), which in both cases resulted in the defective CE.

The results in Fig. 5A-D suggest that TTLL11-mediated polyglutamylation of DVL is required for CE in *Xenopus*. Polyglutamylated DVL3 binds specifically KATNAL2 and RAB11FIP5 (see Fig. 4). In order to test whether these downstream effectors also participate in CE, we have turned into zebrafish *Danio rerio* as a model. We have knocked out fish *Rab11fip5a*, *Rab11fip5-like*, and *Katnal2* genes as well as *Ttll11* by Crispr/Cas9 in zebrafish embryos (**Fig. 5E**) (*45*). Embryos upon deletion of *Rab11fip5a* and *Katnal2* showed body axis truncation phenotypes reminiscent of a defect in the PCP pathway (KO of *Wnt5b* served as the positive control) (**Fig. S7H**). This was further validated by quantitative analysis of the somite length at 14.5 hpf (**Fig. 5F**).

Altogether, these results suggested that polyglutamylated xDvl3 is more potent than xDvl3 WT in the activation of the Wnt/PCP pathway during CE movement. Consistently, downregulation of TTLL11 led to severe defects in gastrulation/neurulation on the *Xenopus* model and KO of genes encoding interactors of the polyglutamylated DVL3 *Rab11fip5a* and *Katnal2* affected CE in *Danio rerio*. Collectively, this analysis supports the hypothesis that TTLL11-mediated polyglutamylation of DVL takes place during gastrulation to facilitate DVL-controlled morphogenetic processes such as CE movements.

Polyglutamylation controls liquid-liquid phase separation (LLPS) of DVL3

What can be the biochemical features of DVL3 affected by polyglutamylation? Since DVL3 can form biomolecular condensates via a process of liquid-liquid phase separation (LLPS) (*46*), we have addressed next this possibility. Depending on the extent of

LLPS, DVL3 is distributed either homogeneously in the cytoplasm, or forms phase-separated "puncta" (**Fig. 6A**).

We thus overexpressed DVL3 WT, polyglutamylation mimicking DVL3-12E, as well as the glutamylation defective DVL3 E710A/D714A alone, or together with WT or ligase-dead TTLL11 (E531G) in HEK293 cells and analyzed the localization pattern of DVL3. To avoid interference with endogenous DVL proteins that were shown to affect this phenotype (*31*) we have performed this experiment primarily in *DVL1/DVL2/DVL3* triple KO cells (**Fig. 6B;** the same experiment in WT HEK293 cells is provided for reference in **Fig. S8C**). Interestingly, polyglutamylation led to a decrease in DVL3 LLPS propensity, i.e., DVL3-12E was distributed more evenly in the cell cytoplasm compared to DVL3 WT (compare bars 1 and 2 in Fig. 6B). On the contrary, glutamylation-defective DVL3 E710A/D714A localized predominantly into puncta (bar 3, Fig. 6B). Co-expression of TTLL11 further promoted even localization of DVL3 WT and DVL3-12E but not of glutamylation-defective DVL3 E710A/D714A (Fig. 6B, compare bars 4-6 with bars 1-3), which suggested that this phenotypic difference is indeed because of polyglutamylation. In line with this assumption, ligase-dead TTLL11 (E531G) promoted puncta formation and LLPS of DVL3 (Fig. 6B, bars 7-9). However, the downregulation of *TTLL11* by siRNA did not show any effect (**Fig. S8A, B**), pointing towards functional redundancy of TTLL11 with other endogenously present TTLL proteins. To address the effect of polyglutamylation on DVL3 LLPS more directly, we analyzed the dynamics of ECFP-tagged wild-type DVL3, DVL3-12E, and DVL3 E710A/D714A using fluorescence recovery after photobleaching (FRAP) (**Fig. 6C,** raw data in **Fig. S8E**). We have selected cells where DVL3 forms puncta and bleached individual puncta of comparable size (**Fig. 6Ca**) and quantified the signal for 325 seconds. As shown in (**Fig. 6Cb**) polyglutamylated DVL3-12E showed much faster recovery of fluorescence than DVL3 WT or DVL3 E710A/D714A. This suggests that the turnover of polyglutamylated DVL3-12E between LLPS separated puncta and other cytoplasmic pools of DVL3 is increased. This observation agrees with its reduced LLPS propensity. Of note, overexpressed TTLL11 localized in cells rather uniformly to the cytoplasm and filamentous structures (probably MT) (**Fig. 6Da**) when expressed alone. When we co-expressed DVL3 and focused on cells that still show punctate localization of DVL3 (approx. 35% of cells, see Fig. 6B) TTLL11 co-localized with DVL3 in puncta (**Fig. 6Db**). Similar behavior was observed for DVL1 and DVL2 puncta (**Fig. S8D**). This demonstrates that TTLL11 can be actively recruited to the sites where LLPS of DVL3 takes place and as such can regulate it *in situ*. Altogether, this data shows that polyglutamylated DVL3 has a lower tendency to phase-separate and consequently forms more dynamic biomolecular condensates.

Polyglutamylation regulates phosphorylation of DVL3

The best-known regulators of DVL3 LLPS are several kinases – most notably CK1ε (*47*) and centrosomal/ciliary kinases NEK2 and TTBK2 (*20, 22*). These kinases upon binding and phosphorylation of DVL3 dissolve its LLPS condensates, resulting in more even cytosolic distribution of DVL3 (*31*). Interestingly, our interactome analysis (Fig. 4B, C) suggested increased interaction of CK1ε and CK1δ, a kinase closely related to and functionally redundant with CK1ε, with polyglutamylated DVL3. We further validated this observation by an independent approach - co-immunoprecipitation of endogenous CK1ε with overexpressed DVL3 in HEK293 cells was significantly promoted by co-expression with TTLL11 (**Fig. S9A**).

The obvious question then was "Are the polyglutamylation effects reflecting only the higher affinity of polyglutamylated DVL3 for CK1s or does polyglutamylation affect LLPS independently?". We have addressed the possible crosstalk between polyglutamylation and phosphorylation by the analysis of subcellular localization of DVL3 WT, polyglutamylated DVL3-12E, and glutamylation-resistant DVL3 E710A/D714A in the presence of exogenous CK1ε and in the presence of PF670462, the inhibitor of CK1δ and CK1ε. These experiments have been performed again in both *DVL1/DVL2/DVL3* TKO (**Fig. 6E**) and WT HEK293 cells (**Fig. S9F**). In both cases co-expression of CK1ε strongly promoted uniform localization of all DVL3 variants, despite being less efficient in the case of DVL3 E710A/D714A (Fig. 6E). On the other side, CK1 inhibition, despite strongly promoting punctate distribution of DVL3, was not able to fully revert the even localization of DVL3-12E caused by polyglutamylation (Fig. 6E, bar 6). CK1 inhibition was less efficient when DVL3-12E was co-expressed with TTLL11 (see Fig. S8F). We conclude that both phosphorylation and polyglutamylation affect DVL3 LLPS independently, but their combination can be additive *in vivo*.

The observations of the additive effect of DVL3 C-terminal polyglutamylation and CK1ε-mediated phosphorylation raised the possibility that these events are mechanistically connected. To address this, we purified ^{15}N labeled DVL3 C-terminal peptides corresponding to aa 693-716 (C24) and aa 693-716-12E (C24-12E) and analyzed the CK1ε phosphorylation kinetics of individual sites *in vitro* by real-time NMR (**Fig. 6F, G and Fig. S9B-E**). DVL3 polyglutamylation modulates CK1ε-mediated phosphorylation pattern in a qualitative and quantitative manner. In common, both peptides get initially phosphorylated at S709, but only the polyglutamylated variant gets fully phosphorylated at this site due to the much faster kinetics under identical experimental conditions. The rest three sites resident at the C-terminal tail, T695, S697, and S700, are phosphorylated only in the polyglutamylated form of the peptide, although partially. The in vitro data provide evidence that polyglutamylation enhances CK1ε activity and significantly affects the phosphorylation dynamics of the DVL3 C-terminus. These two modifications can thus regulate each other and control DVL functions connected with the phosphorylation of the C-terminus – including regulation of open and closed conformation (*31*), participation in the non-canonical ROR2 signaling (*48*) or release from the centrosome during centriole separation (*22*).

DVL3 polyglutamylation and polyglutamylation-induced changes in LLPS are reversed by CCP6

Polyglutamylation of tubulin can be reversed by deglutamylating enzymes from the CCP protein family (*8-10*). We hypothesized that if polyglutamylation of DVL3 has a biological significance, then a deglutamylation mechanism should exist to control this function. CCPs, which have previously been shown to deglutamylate not only tubulin but also non-tubulin proteins such as myosin light-chain kinase (MLCK), whose C-terminus consists of polyglutamate stretch (*9*), were the most likely candidates for such function. We thus tested CCP1, CCP5, and CCP6 as the best-characterized deglutamylating enzymes. CCP1 and CCP6 are deglutamylases shortening polyE chains (*9*), while CCP5 was proposed to remove γ-linked branching glutamylation points (*9*), albeit it can also remove α-linked glutamates at a slower rate (*49*). As shown in **Fig. 7A**, all three CCP enzymes were localized to the cytoplasm when overexpressed, however at least a fraction was recruited into DVL3 puncta upon DVL3 co-expression. In particular, CCP6 showed almost complete co-

localization with DVL3 in these puncta. This suggests that CCP proteins might be capable of interacting with DVL3.

To evaluate such interactions and the potential deglutamylation activity on DVL3 directly, we co-expressed CCP1, CCP5 and CCP6 together with DVL3 WT, the polyglutamylation-mimicking DVL3-12E, as well as glutamylation resistant DVL3 E710A/D714A (**Fig. 7B**). First, this experiment showed that CCP6 binds DVL3 WT much better than CCP1 and CCP5 (IP: FLAG, WB: GFP). Second, we detected a strong complex between DVL3-12E and CCP5 and CCP6 but not CCP1 (IP: GFP, WB: FLAG). On the other hand, DVL3 E710A/D714A showed weaker interaction with all CCPs. This suggests that the interaction of CCP5 and CCP6 is promoted by the C-terminal polyglutamate sequence of DVL3. Lastly and most importantly, CCP1 and especially CCP6 were able to efficiently reduce polyglutamylation of DVL3-12E (IP: Flag, WB: Poly E), which agrees with their known function of removing C-terminal glutamate residues of a linear peptide chain. By contrast, CCP5, known to preferentially act on polyglutamylation branching points (*9, 49*), was less efficient in deglutamylating DVL3. The role of CCP1 and CCP6 in DVL3 deglutamylation was further confirmed by showing that both enzymes, and in particular CCP6, can efficiently reduce DVL3 polyglutamylation generated by TTLL11 (**Fig. S10A**). This effect is specific and depends on the CCP enzymatic activity, as inactive mutants of both CCPs did not reduce DVL3 polyglutamylation. In summary, we showed that CCP1 and CCP6 can remove polyglutamylation of DVL3, and from the tested CCPs, CCP6 is the most efficient DVL3 deglutamylase. We propose that this specificity is achieved by the combination of its capacity to bind polyglutamylated DVL3 stronger than CCP1, which is also deglutamylating DVL3, and to remove linear polyglutamate chains (in contrast to CCP5, which also binds polyglutamylated DVL3).

Knowing that CCPs can remove polyglutamylation of DVL3 we asked whether they also revert the effects polyglutamylation has on LLPS of DVL3. We analyzed the subcellular localization of WT DVL3 and polyglutamylation-mimicking DVL3-12E after co-expression with CCP1, CCP5 and CCP6 (**Fig. 7C, S10B**). Interestingly, while CCP1 and CCP5 did not significantly change the localization pattern of DVL3, CCP6 was able to promote its punctate phenotype, suggesting it promotes the formation of DVL3 protein condensates. This effect of CCP6 was even more pronounced in the case of DVL3-12E (Fig. 7C, compare bars 5-8). This demonstrates that CCP6 not only deglutamylates DVL3 but also prevents its polyglutamylation-induced cellular phenotype. We conclude that CCP6 acts as an enzyme that removes DVL3 polyglutamylation and counteracts the role of polyglutamylation/TTLLL11-mediated control of DVL3 LLPS.

Discussion

Here we discovered that a key protein of the Wnt signaling pathway, DVL3, is post-translationally polyglutamylated by TTLL11 through a previously unknown and unique mechanism, in which a polyglutamate chain is generated at the α-COOH of the terminal amino acid of the substrate protein. The direct elongation of primary peptide chains by adding a variable number of glutamates substantially increases the breadth of polyglutamylation as a PTM. Further, many more proteins than previously expected can be polyglutamylated, in particular because, as we demonstrated, it can take place at multiple C-terminal amino acids including M, A, E, and S. Moreover, TTLL11 could tolerate big changes at the DVL3 C-terminus – including deletion of C-terminal regions or C-terminal elongation by a stretch of 4 As. We propose that once TTLL11 interacts with its substrate it can behave as a rather promiscuous enzyme. Only one sequence modification completely

prevented polyglutamylation in our hands: the mutation of two acidic residues, E710 and D714 to A, which made the DVL3 C-terminus very hydrophobic. It thus appears that the charge/hydrophilicity of amino acid residues near the C-terminal modification site, rather than the sequence motif or identity of C-terminal amino acid, is important for TTLL11-mediated polyglutamylation. This is in agreement with structural analyses of the catalytic site of TTLL enzymes (*50*) and their recognition domain (*51*) which are both positively charged.

Our discovery opens the exciting possibility that many other proteins get polyglutamylated by this mechanism. This is supported by the observation that overexpression of TTLL11 ((*3*), this study) resulted in multiple poly-E-positive bands on the WB of whole-cell lysates. It remains to be identified if/what are the other substrates of TTLL11 in addition to DVL3, and to what extent can other TTLLs elongate α-carboxyl of other amino acids than glutamate and what are their substrate proteins.

Given that the best-studied substrate of TTLL polyglutamylases is tubulin (*1, 33, 52*), initial insights into the function of polyglutamylation come from studies showing the role of this PTM in the modulation of interactions between microtubules and their interacting proteins, such as the microtubule severing proteins katanin and spastin (*53-55*), or molecular motors (*56*). The identification of DVL3 as a polyglutamylation substrate allowed us to discover previously unknown, distinct functions of polyglutamylation, such as the control of protein phosphorylation and of LLPS – two processes that are essential for the biology of DVL. Our demonstration that polyglutamylation of DVL3 reduces its capacity to form biomolecular condensates via LLPS (*57*) phenocopies the effects of CK1ε – the established master regulator of DVL biology that controls its role in the Wnt signaling pathways (*47, 58, 59*). These two mechanisms – polyglutamylation and phosphorylation of DVL3 – probably act in parallel and are mutually supportive as CK1ε binds stronger to polyglutamylated DVL3 and polyglutamylated C-terminus of DVL3 gets phosphorylated by CK1ε much more efficiently.

Polyglutamylation of DVL3, similarly to CK1ε-induced DVL3 phosphorylation, reduced the capacity of this protein to phase-separate and resulted in a more even distribution of DVL3 in cells. In the case of DVL3 phosphorylation, it was shown earlier that decreased LLPS correlated with the "open" conformation of DVL3 (*31*), which is formed when binding of the DVL3 C-terminus to its own PDZ domain is prevented. Intriguingly, the binding of the DVL3 C-terminus to its PDZ domain is mediated by α-carboxyl of M716 (*31, 60*). Thus, it is probable that the polyglutamylation affects the binding of the C-terminus with the PDZ domain both directly, by blocking of M716 α-carboxyl and indirectly by promoting phosphorylation of the C-terminus by CK1ε. Interestingly, it was shown in *Xenopus* embryos that the addition of the C-terminal tag to DVL, which is expected to lead to the open conformation, is mechanistically similar to polyglutamylation promoted the activity of DVL in Wnt/PCP but not Wnt/β-catenin (*32*). This is in perfect agreement with our observations and suggests that TTLL enzymes mediating physiological polyglutamylation can function as important regulators of CE during embryonal development. Peak expression of xTTLL11 at the onset of gastrulation as well as known functions of several proteins that specifically interact with polyglutamylated DVL3 support this possibility. In addition to CK1ε with the known role in the Wnt/PCP pathway (*59, 61, 62*), also two other top hits, namely KATNAL2 and RAB11FIP5, affected CE in *Danio rerio* development. KATNAL2 has a role in microtubule severing and its knockdown in *Xenopus* embryos led to defects in CE including blastopore and neural tube closure (*63*). Moreover, the same study showed that KATNAL2 is expressed in neurogenic tissues and subcellularly localized to the basal body, ciliary axoneme, centriole, and mitotic

spindle. RAB11FIP5, a RAB11 effector involved in apical endosome recycling pathway phenocopied Wnt11 in *Xenopus*, whereas its loss resulted in CE defects (*64*). Interestingly, RAB11FIP5 was shown to be necessary for the ciliary import of polyglutamylase TTLL5 among other signaling molecules (*65*). This indirect evidence suggests that TTLL-mediated polyglutamylation can integrate multiple stimuli required for proper onset of activation of Wnt/PCP during gastrulation. However, the identification of the responsible TTLL enzymes can be challenging due to redundancy among individual TTLL family members that has also large variability across different species. For example, downregulation of TTLL11 exhibited severe phenotype in *Xenopus*, while no phenotype was observed in *Danio rerio*. Similarly, TTLL11 KO mice generated and phenotyped by the IMPC consortium (see https://www.mousephenotype.org/data/genes/MGI:1921660; (*66*)) did not show any obvious phenotype; likely due to redundancy described earlier for example for TTLL4 and TTLL6 (*67*).

One of the key functions of DVL is its role in the basal body and centrosome – summarized in (*68*), where TTLL11 (*3*), as well as CCPs, including CCP6 (*69*) are also localized. Release of DVL3 from the centrosome is controlled by a centrosomal kinase NEK2 (*22*) that phosphorylates multiple S/T residues including C-terminal S697 and S700 and at the same time blocks LLPS of DVL3 (*20*). Given the fact that centrosome and pericentriolar matrix (PCM) is perceived as the phase separated organelle (*70*), and with the observation of DVL biomolecular condensates in the centrosome (*28*) and the role of polyglutamylation in DVL LLPS described here, it will be exciting to explore to which extent polyglutamylation of non-tubulin proteins could, together with centrosomal kinases, control the dynamics of PCM clients via regulation of their LLPS propensity (*71*). Moreover, our study further points to another yet underappreciated crosstalk between phosphorylation and polyglutamylation that is likely to be most relevant in centrosomes and cilia - as hinted by the recent report describing the regulation of centrosomal/ciliary TTLL4 by the centrosomal kinase NEK5 (*72*).

In summary, we here discovered polyglutamylation via α-carboxyl of amino acid other than glutamate, which can effectively lead to the C-terminal linear elongation of primary peptide chains of a substrate. The minimal sequence requirements of the modification site make C-terminal polyglutamylation a potentially versatile PTM with a broad range of substrates. Studying the impact of C-terminal polyglutamylation of the signaling protein DVL3, we discovered functions of polyglutamylation in Wnt/PCP signaling pathway by the regulation of protein phosphorylation and formation of protein condensates via LLPS. Given the biochemical nature of polyglutamylation that allows for gradual charge and signal modulation - a regulatory principle so far only demonstrated for microtubule severing (*53-55*) - we propose that polyglutamylation could play a unique role in fine-tuning of multiple LLPS processes.

Materials and Methods

Cell culture and recombinant Wnt treatment

HEK293T (ATCC-CRL-11268), hTERT RPE-1 (kind gift from E. Nigg, Biozentrum, University of Basel, Basel, Switzerland), HEK293 T-REx DVL1-2-3$^{-/-}$ and HEK293 T-REx DVL1-2-3$^{-/-}$/RNF43$^{-/-}$/ZNRF3$^{-/-}$ (*43, 73*) were grown at 37 °C and 5% CO_2 in complete DMEM medium containing 10% fetal bovine serum (DMEM; Gibco #41966-029), 2mM L-glutamine (Life Technologies, #25030024), 50U/ml penicillin, and 50U/ml streptomycin (Hyclone-Biotech, #SV30010). Cell passaging of adherent cell lines was performed using trypsin (Biosera). The cells were washed in Phosphate Buffered Saline

(PBS) buffer prior to the passage. For protein purification, suspension culture of FreeStyle™ 293-F Cells (Thermo Fisher Scientific) was cultured in FreeStyle™ 293 expression medium (Thermo Fisher Scientific) at 37 °C and 5% CO_2 while shaking at 120 rpm in Erlenmeyer cell culture flasks (Corning). For peptide purification see below - Peptide cloning, expression, and purification. Treatment by recombinant Wnt3a and Wnt5a was performed as follows: HEK293T cells were treated with 1 μM Porcupine inhibitor LGK974 (Stem RD, #974-02) at the time of seeding and was maintained in the media whole time. Cells were transfected by corresponding vectors and 24h post-transfection medium was supplemented with 100ng/ml Wnt3a or Wnt5a (#1324-WN and #645-WN; R&D Systems) and cells were harvested after 3-hour treatment.

Transient Transfection

List of plasmids used in this study is available in **Supplementary table S2**. Adherent cells were seeded with density of 30000 cells per cm^2 if not indicated otherwise (in case of immunocytochemical methods the density was 10000 cells per cm^2). They were incubated for 24 h and transfected using Polyetylenimin (PEI) with stock concentration of 1 mg/ml and pH 7, 4. The amount of PEI and DNA as well as incubation time of cells with transfection mixture differed according to experiment **Supplementary table S3**. DNA and PEI were separately mixed with serum-free DMEM, incubated for 20 min at room temperature (RT) and subsequently mixed. Each mixing step was followed by vortexing and centrifugation. The final mix was incubated for 20 min at RT and added to the cells. A medium was replaced with the fresh complete DMEM after four-hour-long incubation with transfection mixture. The cells were harvested or fixed 24 hours after transfection. Suspension FreeStyle™ 293-F cells were transfected in 200ml culture with density of $4x10^6$ cells per 1ml. 400μg DNA was diluted in 7ml of PBS, while 1.2ml of PEI (1 mg/ml) was diluted in 3ml of PBS. Both mixtures were incubated for 20 min and subsequently mixed and incubated for another 20 min before adding to cell culture. 200ml of fresh media was added to the culture 4 h post-transfection.

Dual luciferase assay for analysis of Wnt/β-catenin signaling

Dual-Luciferase® Reporter Assay System (Promega) was performed by two reporter vectors. The test reporter vector (Super8X TopFlash) contained a gene for firefly luciferase controlled by the promoter containing TCF4-binding repeats. TCL/LEF together with β-catenin are co-activating subsequent transcription. The control reporter (pRLtkLuc) contained the gene for Renilla luciferase with constitutively active promoter. Therefore, an activity of control reporter was used to normalize data for cell viability and transfection variability. The HEK293T cells were seeded on a 24-well plate and transfected according to Supplementary table S3. For rescue experiment (Fig. S6C) cells were treated with 1 μM Porcupine inhibitor LGK974 (Stem RD, #974-02) at the time of seeding. For Wnt stimulation, 200 μl of Wnt3a conditioned medium per condition was used in total 500 μl of medium per well for 14 h (as described in (*43*)). The cells were lysed after 24h incubation (or 14h in case of rescue experiment Fig S6C) and processed following a manufacturer's instructions. Luminescence was measured on MLX luminometer (Dynex Technologies).

Site-directed mutagenesis and cloning

The Twin-Strep-Flag-HALO-DVL3 wt plasmid was made by Gateway Technology (via LR recombination according to the manufacturer's instructions; Thermo Fisher Scientific, #11791020) from the donor plasmid pDONR221 DVL3 (DNASU, #FLH178665.01x) and the destination plasmid pDEST-Twin-Strep-Flag-HALO (kind gift from Cyril Bařinka). The Twin-Strep-Flag-ECFP-DVL3 wt was made as follows: pdECFP-DVL3 (*31*) vector was used as template for PCR product that was inserted into pDONR221,

resulting in pDONR221-ECFP-DVL3 vector that was combined with pDEST-Twin-Strep-Flag-HALO via Gateway Technology (Thermo Fisher Scientific #11791020). HALO tag was subsequently removed by site-directed mutagenesis. Mutagenesis of pcDNA3.1-Flag-hDVl3, Twin-strep-Flag-HALO-DVL3 or pCS2+xDvl3 vector was performed using QuikChange II XL Site-Directed Mutagenesis Kit (Agilent Technologies) following a manufacturer's instructions. Some vectors were made by serial mutagenesis as shown in Supplementary table S3. The PCR was performed using gradient thermal cycler (Bio-Gener Technology). For a bacterial transformation, One Shot® TOP10 Chemically Competent E. coli (Invitrogen) and Super Optimal Broth (SOC) medium were used (Thermo Fisher Scientific). The primers designed for mutagenesis reactions are listed in **Supplementary table S4**. All mutations were verified using Sanger sequencing. For peptide cloning see below - Peptide cloning, expression, and purification.

Co-immunoprecipitation

The HEK293T cells were grown at 10cm dishes to 60 –70% confluency. They were transfected with desired vectors and incubated for 24 h post-transfection. The following work was performed at 4 °C. Cells were lysed for 20 min in 1ml of lysis buffer (50mM Tris, pH=7.4, 150mM NaCl, 1mM EDTA, 0.5% NP 40) supplemented by 1 mM DTT (Sigma-Aldrich) and 1x protease inhibitors (Roche Applied Science). Crude cell lysate was cleared by centrifugation for 15 min at 16000 g. The 80 µl of total cell lysate (TCL) was mixed with 20 µl of 5x Laemmli buffer. Remaining supernatant was divided into samples and each sample was incubated overnight with 1µl of corresponding antibody. G-protein coupled sepharose beads (GE Healthcare) were pre-washed in lysis buffer and blocked overnight in the lysis buffer with 1% BSA. The next day, lysates were combined with 15 µl of the pre-washed G-protein coupled sepharose beads. The mixture was incubated on carousel for 4 hours. After the incubation, the beads were washed 5x in lysis buffer and proteins were eluted by addition of Laemmli buffer to total volume of 80 µl. Used antibodies are listed in the **Supplementary table S5**.

Western blotting

For WB, the samples were incubated at 95°C for 5 min and subjected to SDS-PAGE, then electrotransferred onto Hybond-P membrane (GE Healthcare), immunodetected using appropriate primary and secondary antibodies (conjugated with HRP) and visualized by ECL (Millipore) and documented using FusionSL system (Vilber-Lourmat). WB signal intensities were quantified using ImageJ. Area of the peak intensity for the protein of interest was divided by corresponding values of peaks intensity obtained for control protein. Used antibodies and corresponding dilutions are listed in the Supplementary table S5.

Immunofluorescence

The HEK293T cells were seeded onto 13mm coverslips, coated in 0.1% gelatin. Next day, the cells were transfected with vectors according to the design of experiments or/and treated by 1µM PF670462 (DC chemicals, #DC2086), and subsequently incubated for 24 hours. Then, cells were washed in PBS, fixed in 4% paraformaldehyde (PFA, Millipore) in PBS for 1 hour followed by three washes in PBS and finally blocked in PBTA (PBS, 5% donkey serum, 0.3% Triton X-100, 1% BSA). Samples were incubated overnight at 4°C with primary antibodies diluted in PBTA. Following 3 washes in PBS, samples were incubated with corresponding Alexa Fluor secondary antibodies (Invitrogen, Abcam) for 1h at RT, followed by 5 min incubation at RT with DAPI (Thermo Fisher) for nucleolar staining. Finally, samples were mounted in DAKO KO mounting solution (DAKO KO). The images were taken using fluorescent (Olympus IX51) or confocal (Leica SP8) microscope using ×40 water or ×60 oil objectives. For protein subcellular localization

experiments, at least 200 positive cells per experiment (n = 3) were analyzed and scored according to their phenotype into two categories (puncta/even). Used antibodies and corresponding dilutions are listed in supplementary table S5.

FRAP

RPE cells were seeded to µ-Slide 8 Well (Ibidi) chambers at density 10000 cells per cm^2 24 hours prior to transfection. Cells were transfected with corresponding plasmids of ECFP tagged DVL3 construct (Supplementary table S2 and S3) and incubated another 24 h. Live cell imaging and photobleaching was performed on Zeiss LSM 880 microscope equipped with thermostat and CO_2 chamber using Plan-Apochromat 63x objective. After transferring of cells into the microscope, they were left for 30 minutes to rest. Then, protein condensates of similar size were bleached using 458nm laser and images were taken every 5 seconds. Only condensates that stayed in the plane of focus were considered for analysis. Raw images were processed using ImageJ software using jay plugins (https://github.com/jayunruh/Jay_Plugins) from Jay Unruh at Stowers Institute for Medical Research in Kansas City, MO. Plugins used: create spectrum jru v1, combine all trajectories jru v1, normalize trajectories jru v1 (Min_Max normalization), batch FRAP fit jru v1 and average trajectories jru v1; all using default settings.

LC-MS analysis of polyglutamylated DVL

Selected 1D gel bands were excised manually and after destaining and washing procedures each band was subjected to protein reduction (10mM DTT in 25mM NaHCO3, 45 min, 56°C, 750 rpm) and alkylation (55mM IAA in 25mM NaHCO3; 30 min, laboratory temperature, 750 rpm). After further washing by 50% ACN/$NaHCO_3$ and pure ACN, the gel pieces were incubated with 125 ng trypsin (sequencing grade; Promega) in 50mM $NaHCO_3$. The digestion was performed for 2 h at 40 °C on a Thermomixer (750 rpm; Eppendorf). Tryptic peptides were extracted info LC-MS vials by 2.5% formic acid (FA) in 50% ACN with addition of polyethylene glycol (20,000; final concentration 0.001%, Stejskal et al., 2013) and concentrated in a SpeedVac concentrator (Thermo Fisher Scientific). Additional digestion of selected tryptic digests was conducted by adding 5.2 nmol of CNBr to a vacuum-dried digest reconstituted in 0.5M HCl (16 h, 25°C, 750 rpm).

LC-MS/MS analyses of peptide mixtures coming from in-gel digestions were done using RSLCnano system (Thermo Fisher Scientific) on-line connected to Impact II Qq-Time-Of-Flight mass spectrometer (Bruker, Bremen, Germany). Prior to LC separation, tryptic digests were online concentrated and desalted using trapping column (100 µm × 30 mm, 40°C) filled with 3.5-µm X-Bridge BEH 130 C18 sorbent (Waters, Milford, MA, USA). After washing of trapping column with 0.1% FA, the peptides were eluted (flow 300 nl/min) from the trapping column onto an Acclaim Pepmap100 C18 column (3 µm particles, 75 µm × 500 mm, 40°C; Thermo Fisher Scientific, Waltham, MA, USA) by 50 min nonlinear gradient program (1-56% of mobile phase B; mobile phase A: 0.1% FA in water; mobile phase B: 0.1% FA in 80% acetonitrile). The analytical column outlet was directly connected to the CaptiveSpray nanoBooster ion source (Bruker). NanoBooster was filled with acetonitrile and nanoBooster pressure was set to 0.2 Bar.

MS data were acquired in a data-dependent strategy with 3s long cycle time. Mass range was set to 150-2200 *m/z* and precursors were selected from 300-2000 *m/z*. Acquisition speed of MS and MS/MS scans was 2Hz and 4-16Hz, respectively. Default CID collision energies and isolation widths with respect to precursor charge and *m/z* were used.

Under equivalent ionization and fragmentation conditions, peptide standards at a concentration 0.01 mg/ml (in 50% ACN, 0.1% FA) were directly injected at 3 µl/min flow rate to the ion source by using a syringe pump.

The processing of the mass spectrometric data including recalibration, compounds detection, charge deconvolution and further MS/MS data analysis was carried out in DataAnalysis software (4.2 SR1; Bruker). Mascot MS/MS ion searches (Matrixscience, London, UK; version 2.5.1) were done against in-house database containing expected protein sequences extended with polyE motifs added to the protein C-term or introduced into the sequence after sites tentatively forming side chains. cRAP contaminant database (downloaded from http://www.thegpm.org/crap/) was searched in advance to exclude contaminant spectra prior the main database search. Mass tolerance for peptides and MS/MS fragments were 10 ppm and 0.1 Da, respectively, with the option of one 13C atom to be present in the parent ion. Oxidation of methionine, carbamidomethylation (C), deamidation (N, Q) were set as optional modifications. In case of CNBr digests, methionine modification to homoserine or homoserine lactone was also allowed. All searches were done without enzyme specificity. Presence of modified C-terminal peptides was verified by checking the corresponding extracted ion chromatograms (± 0.015 *m/z*) and by manual verification of the MS/MS data obtained. The mass spectrometry proteomics data have been deposited to the ProteomeXchange Consortium via the PRIDE (*74*) partner repository with the dataset identifier PXD034237.

LC-MS analysis of protein complexes

LC-MS/MS analyses of all peptide mixtures were done using RSLCnano system connected to Orbitrap Fusion Lumos mass spectrometer (Thermo Fisher Scientific). Prior to LC separation, tryptic digests were online concentrated and desalted using trapping column (100 µm × 30 mm) filled with 3.5-µm X-Bridge BEH 130 C18 sorbent (Waters). After washing of trapping column with 0.1% FA, the peptides were eluted (flow rate - 300 nl/min) from the trapping column onto an analytical column (Acclaim Pepmap100 C18, 3 µm particles, 75 µm × 500 mm; Thermo Fisher Scientific) by 100 min nonlinear gradient program (1-56% of mobile phase B; mobile phase A: 0.1% FA in water; mobile phase B: 0.1% FA in 80% ACN). Equilibration of the trapping column and the column was done prior to sample injection to sample loop. The analytical column outlet was directly connected to the Digital PicoView 550 (New Objective) ion source with sheath gas option and SilicaTip emitter (New Objective; FS360-20-15-N-20-C12) utilization. ABIRD (Active Background Ion Reduction Device, ESI Source Solutions) was installed (*43*).

MS data were acquired in a data-dependent strategy with cycle time for 3 seconds and with survey scan (350-2000 m/z). The resolution of the survey scan was 60000 (200 m/z) with a target value of 4×105 ions and maximum injection time of 50 ms. HCD MS/MS (30% relative fragmentation energy, normal mass range) spectra were acquired with a target value of 5.0x104 and resolution of 30 000 (200 m/z). The maximum injection time for MS/MS was 50 ms. Dynamic exclusion was enabled for 60 s after one MS/MS spectra acquisition. The isolation window for MS/MS fragmentation was set to 1.6 m/z (*75*).

The analysis of the mass spectrometric RAW data files was carried out using the MaxQuant software (version 1.6.0.16) using default settings unless otherwise noted. MS/MS ion searches were done against modified cRAP database (based on http://www.thegpm.org/crap) containing protein contaminants like keratin, trypsin etc., and UniProtKB protein database for Homo Sapiens (https://ftp.uniprot.org/pub/databases/uniprot/current_release/knowledgebase/reference_proteomes/Eukaryota/UP000005640/UP000005640_9606.fasta.gz; downloaded 22.11.2017,

version 2017/11, number of protein sequences: 21,009). Oxidation of methionine and proline, deamidation (N, Q) and acetylation (protein N-terminus) as optional modification, and trypsin/P enzyme with 2 allowed miscleavages were set. Peptides and proteins with FDR threshold <0.01 and proteins having at least one unique or razor peptide were considered only. Match between runs was set among all analyzed samples. Protein abundance was assessed using protein intensities calculated by MaxQuant (*75*). The mass spectrometry proteomics data have been deposited to the ProteomeXchange Consortium via the PRIDE (*74*) partner repository with the dataset identifier PXD033548.

Interactome analysis

Protein intensities reported in proteinGroups.txt file (output of MaxQuant) were further processed using the software container environment (https://github.com/OmicsWorkflows), version 3.7.2a. Processing workflow is available upon request. Briefly, it covered: a) removal of decoy hits and contaminant protein groups, b) protein group intensities $\log_2$ transformation, c) LoessF normalization, d) imputation by the global minimum and e) differential expression using LIMMA statistical test. Volcano plot was created in R version 3.6.1, using the log fold change and adjusted p-value reported by LIMMA. Proteins passing the threshold of log fold change >1 and adjusted p-value < 0.05 were further processed by REPRINT with integrated CRAPOME and SAINTexpress tools. For the background list of contaminants, CC66 was used; SAINTexpress was run with the default settings only against the CRAPOME control. REPRINT output was further processed by ProHits-Viz web interface producing Dot Plots and Correlation heat maps using default settings. Scripts to reproduce analyses are available at Zenodo https://doi.org/10.5281/zenodo.7231808.

Recombinant protein purification

Full-length DVL3 wt, DVL3-E, DVL3 DCA (E710A/D714A) and TTLL11 (212-800) were produced as described in (31) with minimal changes: Twin-Strep-Flag-HALO N-terminally tagged DVL3 or TTLL11 were expressed in HEK293 cells using transient transfection. Cells were harvested 48 h post-transfection, resuspended in a lysis buffer (50 mM Tris pH 8, 150 mM NaCl, 10 mM KCl, 10%glycerol) with cocktail of protease inhibitors (#11836145001, Roche) and 0.2% NP40 (#74385, Sigma). The mixture was incubated for 20 min on ice and cell lysis was enhanced by dounce. Cell lysate was cleared by centrifugation at 100,000g for 45 min at 4 °C and supernatant was loaded on Strep-Tactin Superflow high-capacity column (#2-1237-001, IBA) equilibrated in the lysis buffer. The column was washed in lysis buffer and the protein was eluted using lysis buffer supplemented with 3 mM desthiobiotin. Eluted proteins were concentrated to 0.5 mg/ml using protein concentrators (#88516; Thermo Fisher Scientific), flash frozen in liquid nitrogen, and aliquots were stored at−80 °C. Tubulin and assembled MT were prepared as previously described (*76*).

Peptide cloning, expression, and purification.

pET vectors expressing C-terminal peptides of Dvl3 (C24 or C24-12E) were constructed using annealed oligo cloning. Complementary oligonucleotides were designed to create a double stranded fragment with 5' overhangs compatible with NcoI and KpnI restriction enzymes sites. Overlapping oligonucleotides were annealed, phosphorylated at 5'-termini by T4 Polynucleotide Kinase (M0201, New England Biolabs) and ligated using T4 DNA Ligase (M0202, New England Biolabs) to the pET vector digested with the same restriction enzymes. Finally, the expression constructs of the following form were obtained: His_6 – ZZ tag – TEV cleavage site – peptide sequence. Peptides were expressed in *E. coli* BL21(DE3) strain (C2527I, New England Biolabs) and grown in M9 medium for ^{15}N

794 labeling. The expression was induced with 0.5 mM IPTG (Alchimica). After cell harvest
795 and lysis, the supernatant was loaded on an IMAC column (HisTrap HP 5 ml, GE
796 Healthcare) in a buffer containing 25 mM Tris pH 8.0, 500 mM NaCl, 10 mM imidazole,
797 5% glycerol and eluted in the same buffer with 500mM imidazole. The eluant was treated
798 with TEV protease (produced in-house) for 1 h at 25 °C to cleave the tag and dialysed for
799 16 h at 4 °C to remove the imidazole. The next day, the sample was boiled, snap cooled and
800 spined at 4,000 g for 20 min at 25 °C before loading to IMAC for tag removal. The flow-
801 through containing the peptide was concentrated by centrifugation (Vivaspin 20, 3,000
802 MWCO PES, Sartorius) and subjected to SEC (Superdex 75 10/300 GL, GE Healthcare) in
803 NMR buffer (50 mM phosphate buffer pH 6.5, 50 mM KCl). Peptides were detected in SEC
804 using low UV wavelength (214 nm). The CK1ε kinase core (1-301) was expressed in LB
805 medium and purified as described before for CK1δ kinase core (*77*).

806 **Nuclear magnetic resonance spectroscopy**.

807 All experiments were recorded at 25 °C. Chemical shift assignment of the ^{15}N-
808 labeled peptides was performed using a combination of ^{15}N-NOESY-HSQC and ^{15}N-
809 TOCSY-HSQC experiments recorded at a 950 MHz Bruker Avance NEO spectrometer.
810 Phosphorylation kinetics were measured using a series of ^{1}H-^{15}N HSQC experiments at a
811 700 MHz Bruker Avance NEO spectrometer. The general sample composition of a real-
812 time phosphorylation measurement was as follows: ^{15}N-labeled peptide (50 µM), ATP (1
813 mM), $MgCl_2$ (10 mM), d_6-EDTA (1 mM), D_2O for lock (10 %), CK1ε kinase core (1 µM;
814 kinase:peptide ratio of 1:50) in NMR buffer up to a final volume of 200 µl. Kinase was
815 added last in the NMR tube and series of ^{1}H-^{15}N HSQC spectra were recorded every 30
816 minutes over a time course of 16 hours.

817 **Nuclear magnetic resonance kinetic analysis.**

818 NMR spectra were analyzed using Sparky 3.115. The fraction of phosphorylation
819 for a given amino acid at a given time point was calculated by dividing the peak intensity
820 of the phosphorylated form by the sum of peak intensities of phosphorylated and non-
821 phosphorylated forms ($I_{phospho}/(I_{phospho} + I_{nonphospho})$). The experimental data were fitted to a
822 mono-exponential function f(x)=A*(1-exp(-k*x)) using Gnuplot 5.2.4.

823 **In-vitro polyglutamylation**

824 DVL3 was mixed with TTLL11 (212-800) in BRB30 Buffer (30mM PIPES, 8mM
825 MgCl2, 1mM EGTA, pH 6.8) supplemented by 4mM ATP, 4mM Glu, 2mM TCEP, 2xPI,
826 1mM EDTA, TEV protease 0.03 mg/ml. Buffer to protein mixture was 1:1. The mixture
827 was either mixed with the sampling buffer or incubated 60 min at 37°C and subsequently
828 mixed with the sampling buffer. The proteins were separated using SDS PAGE and
829 visualized by CBB staining or immunoblotting. MS analysis was performed on the samples
830 from excised bands of interest from CBB stained gel.

831 **Statistics**

832 In graphs, numerical data are shown as mean ± S.D. as depicted. One-way ANOVA
833 with Dunnett` multiple comparisons test was used for dual luciferase assay in Fig S6C. For
834 comparisons of Fold change, One-sample t-test with theoretical mean = 1 was used as
835 samples were normalized to control (= 1) which as a result had zero variability. (*, $p \leq 0.05$;
836 **, $p \leq 0.01$; ***, $p \leq 0.001$; ns, not significant, $p > 0.05$). Indicated statistical test were
837 calculated by GraphPad Prism 9 (GraphPad Software Inc.).

838 For DVL3 subcellular localization experiments, the data on frequencies puncta vs.
839 even were analyzed using linear mixed model fit by REML and Type III ANOVA with

Satterthwaite`s method followed by multiple comparisons of means (Tukey contrast) in R software version 3.6.1 using lme4 and multcomp packages. Other method-specific statistical operations are explained in corresponding method section. Scripts to reproduce analyses are available at Zenodo https://doi.org/10.5281/zenodo.7231808.

Xenopus embryos

The work with *Xenopus laevis* was carried out according to the Czech animal use and care law and approved by the local authorities and committees (Animal Care and Housing Approval: 45055/2020-MZE-18134, issued by Ministry of Agriculture of the Czech Republic; and Animal Experiments Approval: CZ 62760214, issued by State Veterinary Administration/Section for South Moravian Region).

The generation and cultivation of Xenopus embryos were performed following general protocols. In brief, testes from males under anesthesia (20% MS-222, Sigma-Aldrich, #A5040) were removed surgically from the body cavity and transferred to cold 1x Marc's Modified Ringers (MMR; 100mM NaCl, 2mM KCl, 1mM $MgSO_4$, 2mM $CaCl_2$, 5mM HEPES, buffered to pH 7.4) supplemented with 50ug/mL of gentamycin (Sigma-Aldrich, #G3632). To induce egg laying, fully mature Xenopus females were injected with 260 U of human chorionic gonadotropin (hCG; Merck, Ovitrelle 250G) into the dorsal lymph sac about 12-16 h before use and kept overnight at 18 °C. For fertilization, eggs were squeezed from an induced female directly into a petri dish and mixed with a piece of testes in 0.1x MMR. After 20 mins, embryos were dejellying using 3% cysteine solution (Sigma-Aldrich, C7880) buffered to pH 7.8 for circa 10 mins until they contact each other. Washed embryos (5x in 0.1x MMR solution) were cultivated at 16-18 °C for subsequent microinjections of nucleic acids.

The RNA for microinjections was synthesized from the plasmid pCS2 myc-xDvl3 WT and its derivate 12E using the mMessage mMachine SP6 kit (ThermoFisher, #AM1340). xTTLL11 ATG MO (taactttcttatgggcttttcccag) and xTTLL11 splicing MO for exon 3 (tacagaataatgagggccactca) were ordered from Gene tools (https://www.gene-tools.com/). For microinjections, embryos were cultivated in 3% Ficoll PM400 (Cytiva, #17030010) in 0.6x MMR and injected at the four- cell stage into the two dorsal blastomeres with 100pg of myc-xDvl3 RNAs for the analysis of morphogenetic defects. Before gastrulation (stage 10.5), the embryos were cultivated in 0.1x MMR until they reached stage 26, fixed for 2 h in formaldehyde solution 4% buffered to pH 6.9 (Sigma-Aldrich, #100496), and analyzed for morphogenetic defects. Alternatively, five embryos (stage 26) were lysed before fixation in a 5x Laemmli loading buffer for the subsequent SDS- PAGE/WB analysis. As for the analysis of blastopore closure, the embryos were cultivated in 0.1x MMR enriched with 50 ug/mL of gentamycin (Sigma-Aldrich, #G3632). The number of embryos for each condition is indicated below the graphs (created by GraphPad software) and it is representative of 1-3 biological experiments. All embryos were staged after the normal table of Niewkoop and Faber (*78*). The pictures of embryos were taken on plates with 2% agarose (Serva, #11404) using Leica S9i stereoscope and LAX software.

Zebrafish crispants

Oligonucleotide sequences for gRNA production were selected using the web tool https://chopchop.cbu.uib.no (*79*). A protocol published by Shah et al. (*45*) was utilized for gRNA production. A mixture consisting of rCas9NLS protein (0.66 mg/ml, Sigma-Aldrich CAS9PL), Phenol red (0.05%, Sigma-Aldrich P0290), 120 mM KCl, and gRNA (200 ng/µl) was injected in a volume of 1 nl into the cells of one-cell stage embryos of the AB zebrafish strain. In control injections, an equivalent concentration of BSA was used in place of rCAS9 in an otherwise identical mixture. At 14.5 hpf, dechorionated embryos were fixed using 4%

PFA for one hour, followed by three 20-minute washes in PBST (1% Tween in PBS). Subsequently, samples were permeabilized for 10 minutes in 1% Triton X-100 in PBS, washed for 20 minutes in PBST and blocked for 2 hours in 3% BSA in PBST. Following blocking, the myoD1 antibody (Abcam ab209976, 1:400) was added and incubated overnight at 4°C on a slow shaker. Then, samples were washed 3x for 20 minutes in PBST and incubated with a secondary antibody (α-Rabbit Alexa Fluor 488, 1:500) for 2 hours at room temperature. After incubation, a final round of washing was performed. Finally, samples were dissected, mounted on slides, and imaged using a Leica SP8 confocal microscope.

References

1. B. Edde *et al.*, Posttranslational glutamylation of alpha-tubulin. *Science* **247**, 83-85 (1990).
2. C. Janke *et al.*, Tubulin polyglutamylase enzymes are members of the TTL domain protein family. *Science* **308**, 1758-1762 (2005).
3. J. van Dijk *et al.*, A targeted multienzyme mechanism for selective microtubule polyglutamylation. *Mol Cell* **26**, 437-448 (2007).
4. K. K. Mahalingan *et al.*, Structural basis for polyglutamate chain initiation and elongation by TTLL family enzymes. *Nat Struct Mol Biol* **27**, 802-813 (2020).
5. C. Regnard *et al.*, Polyglutamylation of nucleosome assembly proteins. *J Biol Chem* **275**, 15969-15976 (2000).
6. J. van Dijk *et al.*, Polyglutamylation is a post-translational modification with a broad range of substrates. *J Biol Chem* **283**, 3915-3922 (2008).
7. B. Ye *et al.*, Klf4 glutamylation is required for cell reprogramming and early embryonic development in mice. *Nat Commun* **9**, 1261 (2018).
8. Y. Kimura *et al.*, Identification of tubulin deglutamylase among Caenorhabditis elegans and mammalian cytosolic carboxypeptidases (CCPs). *J Biol Chem* **285**, 22936-22941 (2010).
9. K. Rogowski *et al.*, A family of protein-deglutamylating enzymes associated with neurodegeneration. *Cell* **143**, 564-578 (2010).
10. O. Tort *et al.*, The cytosolic carboxypeptidases CCP2 and CCP3 catalyze posttranslational removal of acidic amino acids. *Mol Biol Cell* **25**, 3017-3027 (2014).
11. J. Bilic *et al.*, Wnt induces LRP6 signalosomes and promotes dishevelled-dependent LRP6 phosphorylation. *Science* **316**, 1619-1622 (2007).
12. W. Kan *et al.*, Limited dishevelled/Axin oligomerization determines efficiency of Wnt/β-catenin signal transduction. *Elife* **9**, (2020).
13. H. Clevers, R. Nusse, Wnt/β-catenin signaling and disease. *Cell* **149**, 1192-1205 (2012).
14. M. T. Butler, J. B. Wallingford, Planar cell polarity in development and disease. *Nat Rev Mol Cell Biol* **18**, 375-388 (2017).
15. M. Mlodzik, The Dishevelled Protein Family: Still Rather a Mystery After Over 20 Years of Molecular Studies. *Curr Top Dev Biol* **117**, 75-91 (2016).
16. Y. Peng, J. D. Axelrod, Asymmetric protein localization in planar cell polarity: mechanisms, puzzles, and challenges. *Curr Top Dev Biol* **101**, 33-53 (2012).
17. C. Gao, Y. G. Chen, Dishevelled: The hub of Wnt signaling. *Cell Signal* **22**, 717-727 (2010).
18. J. B. Wallingford, R. Habas, The developmental biology of Dishevelled: an enigmatic protein governing cell fate and cell polarity. *Development* **132**, 4421-4436 (2005).
19. A. Wynshaw-Boris, Dishevelled: in vivo roles of a multifunctional gene family during development. *Curr Top Dev Biol* **101**, 213-235 (2012).

20. K. Hanakova *et al.*, Comparative phosphorylation map of Dishevelled 3 links phospho-signatures to biological outputs. *Cell Commun Signal* **17**, 170 (2019).
21. T. J. Park, B. J. Mitchell, P. B. Abitua, C. Kintner, J. B. Wallingford, Dishevelled controls apical docking and planar polarization of basal bodies in ciliated epithelial cells. *Nat Genet* **40**, 871-879 (2008).
22. I. Cervenka *et al.*, Dishevelled is a NEK2 kinase substrate controlling dynamics of centrosomal linker proteins. *Proc Natl Acad Sci U S A* **113**, 9304-9309 (2016).
23. K. Kikuchi, Y. Niikura, K. Kitagawa, A. Kikuchi, Dishevelled, a Wnt signalling component, is involved in mitotic progression in cooperation with Plk1. *EMBO J* **29**, 3470-3483 (2010).
24. M. Fiedler, C. Mendoza-Topaz, T. J. Rutherford, J. Mieszczanek, M. Bienz, Dishevelled interacts with the DIX domain polymerization interface of Axin to interfere with its function in down-regulating beta-catenin. *Proc Natl Acad Sci U S A* **108**, 1937-1942 (2011).
25. M. V. Gammons, M. Renko, C. M. Johnson, T. J. Rutherford, M. Bienz, Wnt Signalosome Assembly by DEP Domain Swapping of Dishevelled. *Mol Cell* **64**, 92-104 (2016).
26. T. Schwarz-Romond *et al.*, The DIX domain of Dishevelled confers Wnt signaling by dynamic polymerization. *Nat Struct Mol Biol* **14**, 484-492 (2007).
27. T. Schwarz-Romond, C. Metcalfe, M. Bienz, Dynamic recruitment of axin by Dishevelled protein assemblies. *J Cell Sci* **120**, 2402-2412 (2007).
28. A. Schubert *et al.*, Superresolution microscopy localizes endogenous Dvl2 to Wnt signaling-responsive biomolecular condensates. *Proc Natl Acad Sci U S A* **119**, e2122476119 (2022).
29. J. H. Henson, B. Samasa, C. B. Shuster, A. H. Wikramanayake, The nanoscale organization of the Wnt signaling integrator Dishevelled in the vegetal cortex domain of an egg and early embryo. *PLoS One* **16**, e0248197 (2021).
30. S. Z. Swartz *et al.*, Polarized Dishevelled dissolution and reassembly drives embryonic axis specification in sea star oocytes. *Curr Biol* **31**, 5633-5641.e5634 (2021).
31. J. Harnos *et al.*, Dishevelled-3 conformation dynamics analyzed by FRET-based biosensors reveals a key role of casein kinase 1. *Nat Commun* **10**, 1804 (2019).
32. J. Qi *et al.*, Autoinhibition of Dishevelled protein regulated by its extreme C terminus plays a distinct role in Wnt/beta-catenin and Wnt/planar cell polarity (PCP) signaling pathways. *J Biol Chem* **292**, 5898-5908 (2017).
33. V. Redeker, J. P. Le Caer, J. Rossier, J. C. Prome, Structure of the polyglutamyl side chain posttranslationally added to alpha-tubulin. *J Biol Chem* **266**, 23461-23466 (1991).
34. R. E. de Groot *et al.*, Huwe1-mediated ubiquitylation of dishevelled defines a negative feedback loop in the Wnt signaling pathway. *Sci Signal* **7**, ra26 (2014).
35. R. Thazhath, C. Liu, J. Gaertig, Polyglycylation domain of beta-tubulin maintains axonemal architecture and affects cytokinesis in Tetrahymena. *Nat Cell Biol* **4**, 256-259 (2002).
36. C. Janke, M. M. Magiera, The tubulin code and its role in controlling microtubule properties and functions. *Nat Rev Mol Cell Biol* **21**, 307-326 (2020).
37. H. Choi *et al.*, Analyzing protein-protein interactions from affinity purification-mass spectrometry data with SAINT. *Curr Protoc Bioinformatics* **Chapter 8**, Unit8.15 (2012).
38. D. Mellacheruvu *et al.*, The CRAPome: a contaminant repository for affinity purification-mass spectrometry data. *Nat Methods* **10**, 730-736 (2013).
39. M. Sharma, I. Castro-Piedras, G. E. Simmons, K. Pruitt, Dishevelled: A masterful conductor of complex Wnt signals. *Cell Signal* **47**, 52-64 (2018).
40. O. Bernatik *et al.*, Sequential activation and inactivation of Dishevelled in the Wnt/beta-catenin pathway by casein kinases. *J Biol Chem* **286**, 10396-10410 (2011).

41. M. Kishida *et al.*, Synergistic activation of the Wnt signaling pathway by Dvl and casein kinase Iepsilon. *J Biol Chem* **276**, 33147-33155 (2001).
42. K. Tamai *et al.*, A mechanism for Wnt coreceptor activation. *Mol Cell* **13**, 149-156 (2004).
43. P. Paclíková *et al.*, Roles of individual human Dishevelled paralogs in the Wnt signalling pathways. *Cell Signal* **85**, 110058 (2021).
44. H. Hikasa, S. Y. Sokol, Wnt signaling in vertebrate axis specification. *Cold Spring Harb Perspect Biol* **5**, a007955 (2013).
45. A. N. Shah, C. F. Davey, A. C. Whitebirch, A. C. Miller, C. B. Moens, Rapid reverse genetic screening using CRISPR in zebrafish. *Nat Methods* **12**, 535-540 (2015).
46. R. P. Sear, Dishevelled: a protein that functions in living cells by phase separating. *Soft Matter* **3**, 680-684 (2007).
47. V. Bryja, G. Schulte, N. Rawal, A. Grahn, E. Arenas, Wnt-5a induces Dishevelled phosphorylation and dopaminergic differentiation via a CK1-dependent mechanism. *J Cell Sci* **120**, 586-595 (2007).
48. F. Witte *et al.*, Negative regulation of Wnt signaling mediated by CK1-phosphorylated Dishevelled via Ror2. *FASEB J* **24**, 2417-2426 (2010).
49. I. Berezniuk *et al.*, Cytosolic carboxypeptidase 5 removes alpha- and gamma-linked glutamates from tubulin. *J Biol Chem* **288**, 30445-30453 (2013).
50. K. Natarajan, S. Gadadhar, J. Souphron, M. M. Magiera, C. Janke, Molecular interactions between tubulin tails and glutamylases reveal determinants of glutamylation patterns. *EMBO Rep* **18**, 1013-1026 (2017).
51. C. P. Garnham *et al.*, Multivalent Microtubule Recognition by Tubulin Tyrosine Ligase-like Family Glutamylases. *Cell* **161**, 1112-1123 (2015).
52. J. E. Alexander *et al.*, Characterization of posttranslational modifications in neuron-specific class III beta-tubulin by mass spectrometry. *Proc Natl Acad Sci U S A* **88**, 4685-4689 (1991).
53. B. Lacroix *et al.*, Tubulin polyglutamylation stimulates spastin-mediated microtubule severing. *J Cell Biol* **189**, 945-954 (2010).
54. M. L. Valenstein, A. Roll-Mecak, Graded Control of Microtubule Severing by Tubulin Glutamylation. *Cell* **164**, 911-921 (2016).
55. S. C. Shin *et al.*, Structural and Molecular Basis for Katanin-Mediated Severing of Glutamylated Microtubules. *Cell Rep* **26**, 1357-1367.e1355 (2019).
56. M. Sirajuddin, L. M. Rice, R. D. Vale, Regulation of microtubule motors by tubulin isotypes and post-translational modifications. *Nat Cell Biol* **16**, 335-344 (2014).
57. T. Schwarz-Romond, C. Merrifield, B. J. Nichols, M. Bienz, The Wnt signalling effector Dishevelled forms dynamic protein assemblies rather than stable associations with cytoplasmic vesicles. *J Cell Sci* **118**, 5269-5277 (2005).
58. F. Cong, L. Schweizer, H. Varmus, Casein kinase Iepsilon modulates the signaling specificities of dishevelled. *Mol Cell Biol* **24**, 2000-2011 (2004).
59. J. M. Peters, R. M. McKay, J. P. McKay, J. M. Graff, Casein kinase I transduces Wnt signals. *Nature* **401**, 345-350 (1999).
60. H. J. Lee, D. L. Shi, J. J. Zheng, Conformational change of Dishevelled plays a key regulatory role in the Wnt signaling pathways. *Elife* **4**, e08142 (2015).
61. R. M. McKay, J. M. Peters, J. M. Graff, The casein kinase I family in Wnt signaling. *Dev Biol* **235**, 388-396 (2001).
62. V. Bryja *et al.*, Beta-arrestin and casein kinase 1/2 define distinct branches of non-canonical WNT signalling pathways. *EMBO Rep* **9**, 1244-1250 (2008).
63. H. R. Willsey *et al.*, Katanin-like protein Katnal2 is required for ciliogenesis and brain development in Xenopus embryos. *Dev Biol* **442**, 276-287 (2018).

64. V. Wallkamm *et al.*, Regulation of distinct branches of the non-canonical Wnt-signaling network in Xenopus dorsal marginal zone explants. *BMC Biol* **14**, 55 (2016).
65. K. He *et al.*, Axoneme polyglutamylation regulated by Joubert syndrome protein ARL13B controls ciliary targeting of signaling molecules. *Nat Commun* **9**, 3310 (2018).
66. M. E. Dickinson *et al.*, High-throughput discovery of novel developmental phenotypes. *Nature* **537**, 508-514 (2016).
67. M. Casanova *et al.*, Characterisation of polyglutamylases in trypanosomatids. *Int J Parasitol* **45**, 121-132 (2015).
68. V. Bryja, I. Červenka, L. Čajánek, The connections of Wnt pathway components with cell cycle and centrosome: side effects or a hidden logic? *Crit Rev Biochem Mol Biol* **52**, 614-637 (2017).
69. M. Rodríguez de la Vega Otazo, J. Lorenzo, O. Tort, F. X. Avilés, J. M. Bautista, Functional segregation and emerging role of cilia-related cytosolic carboxypeptidases (CCPs). *FASEB J* **27**, 424-431 (2013).
70. D. Zwicker, M. Decker, S. Jaensch, A. A. Hyman, F. Jülicher, Centrosomes are autocatalytic droplets of pericentriolar material organized by centrioles. *Proc Natl Acad Sci U S A* **111**, E2636-2645 (2014).
71. J. B. Woodruff *et al.*, The Centrosome Is a Selective Condensate that Nucleates Microtubules by Concentrating Tubulin. *Cell* **169**, 1066-1077.e1010 (2017).
72. T. D. Melo-Hanchuk, J. Kobarg, Polyglutamylase activity of tubulin tyrosine ligase-like 4 is negatively regulated by the never in mitosis gene A family kinase never in mitosis gene A -related kinase 5. *World J Biol Chem* **12**, 38-51 (2021).
73. P. Paclíková, O. Bernatík, T. W. Radaszkiewicz, V. Bryja, The N-Terminal Part of the Dishevelled DEP Domain Is Required for Wnt/β-Catenin Signaling in Mammalian Cells. *Mol Cell Biol* **37**, (2017).
74. Y. Perez-Riverol *et al.*, The PRIDE database resources in 2022: a hub for mass spectrometry-based proteomics evidences. *Nucleic Acids Res* **50**, D543-D552 (2022).
75. S. Tanasa *et al.*, A complex role of Arabidopsis CDKD;3 in meiotic progression and cytokinesis. *bioRxiv*, 2022.2008.2008.503215 (2022).
76. L. Skultetyova *et al.*, Human histone deacetylase 6 shows strong preference for tubulin dimers over assembled microtubules. *Sci Rep* **7**, 11547 (2017).
77. A. Long, H. Zhao, X. Huang, Structural basis for the interaction between casein kinase 1 delta and a potent and selective inhibitor. *J Med Chem* **55**, 956-960 (2012).
78. P. D. Nieuwkoop, J. Faber, *Normal table of Xenopus laevis (Daudin) : a systematical and chronological survey of the development from the fertilized egg till the end of metamorphosis*. (Routledge, New York, 1994), pp. 252 s., 210 s. obr. příl.
79. K. Labun *et al.*, CHOPCHOP v3: expanding the CRISPR web toolbox beyond genome editing. *Nucleic Acids Res* **47**, W171-W174 (2019).
80. D. V. Tauriello *et al.*, Loss of the tumor suppressor CYLD enhances Wnt/beta-catenin signaling through K63-linked ubiquitination of Dvl. *Mol Cell* **37**, 607-619 (2010).
81. M. Narimatsu *et al.*, Regulation of planar cell polarity by Smurf ubiquitin ligases. *Cell* **137**, 295-307 (2009).
82. S. Angers *et al.*, The KLHL12-Cullin-3 ubiquitin ligase negatively regulates the Wnt-beta-catenin pathway by targeting Dishevelled for degradation. *Nat Cell Biol* **8**, 348-357 (2006).
83. M. T. Veeman, D. C. Slusarski, A. Kaykas, S. H. Louie, R. T. Moon, Zebrafish prickle, a modulator of noncanonical Wnt/Fz signaling, regulates gastrulation movements. *Curr Biol* **13**, 680-685 (2003).

84. S. Foldynová-Trantírková *et al.*, Breast cancer-specific mutations in CK1epsilon inhibit Wnt/beta-catenin and activate the Wnt/Rac1/JNK and NFAT pathways to decrease cell adhesion and promote cell migration. *Breast Cancer Res* **12**, R30 (2010).
85. K. Seitz *et al.*, β-Arrestin interacts with the beta/gamma subunits of trimeric G-proteins and dishevelled in the Wnt/Ca(2+) pathway in xenopus gastrulation. *PLoS One* **9**, e87132 (2014).

Acknowledgments

Funding:
Czech Science Foundation grant GX19-28347X (VB)
French National Research Agency grant ANR-10-IDEX-0001-02 (CJ)
LabEx Cell'n'Scale grant ANR-11-LBX-0038 (CJ)
Institut de convergence Q-life grant ANR-17-CONV-0005 (CJ)
French National Research Agency grant ANR-12-BSV2-0007 (CJ)
French National Research Agency grant ANR-17-CE13-0021 (CJ)
Czech Academy of Sciences grant RVO: 86652036 (CB)
Czech Science Foundation (Project GA22-25365S) (CB)
Czech Science Foundation (Project GA22-06405S) (JH)
Charles University Grant Agency (project no. 1414120) (JN)

We acknowledge the core facility CELLIM supported by the Czech-BioImaging large RI project (LM2018129 funded by MEYS CR) for their support with obtaining scientific data presented in this paper. CIISB research infrastructure project LM2018127 funded by MEYS CR and European Regional Development Fund-Project „UP CIISB" (No. CZ.02.1.01/0.0/0.0/18_046/0015974 are gratefully acknowledged for the financial support of the measurements at the Proteomics Core Facility (CEITEC) and at the Josef Dadok National NMR Centre. Computational resources were supplied by the project "e-Infrastruktura CZ" (e-INFRA LM2018140) provided within the program Projects of Large Research, Development and Innovations Infrastructures.

We would like to thank Bryjalab members and Mikołaj Nowak (Institut Curie) for technical support.

Author contributions:

Conceptualization: MK, VB, IČ
Methodology: MK, OŠ, KG, DP, VB, JH
Formal analysis: MK, OŠ, KG, DP, MM, MŠ, RG, NZ
Investigation: MK, OŠ, DP, JN, MM, MŠ, NZ
Visualization: MK, MŠ
Supervision: VB, KT, JH, CB, ZZ, CJ
Resources: CJ, CB
Writing—original draft: MK, VB
Writing—review & editing: VB, MK, CJ, IČ, JN, CB OŠ, KG, ZZ

Competing interests: The authors declare that they have no competing interests.

Data and materials availability: All data needed for evaluation of the study (apart from raw mass spectrometry datasets) are present in the paper and/or in the Supplementary Material. The mass spectrometry proteomics data have been deposited to the ProteomeXchange Consortium via the PRIDE partner repository with the dataset identifier PXD034237 and PXD033548 for LC-MS analysis of DVL3 polyglutamylation and DVL3

interactome, respectively. Scripts to reproduce analyses are available at Zenodo https://doi.org/10.5281/zenodo.7370985. All reagents used are mentioned in Materials and Methods section or listed in supplementary material with corresponding source and/or RRID. Unique reagents generated in this study (plasmids, recombinant proteins) are available upon request.

Figures and Tables

Fig. 1

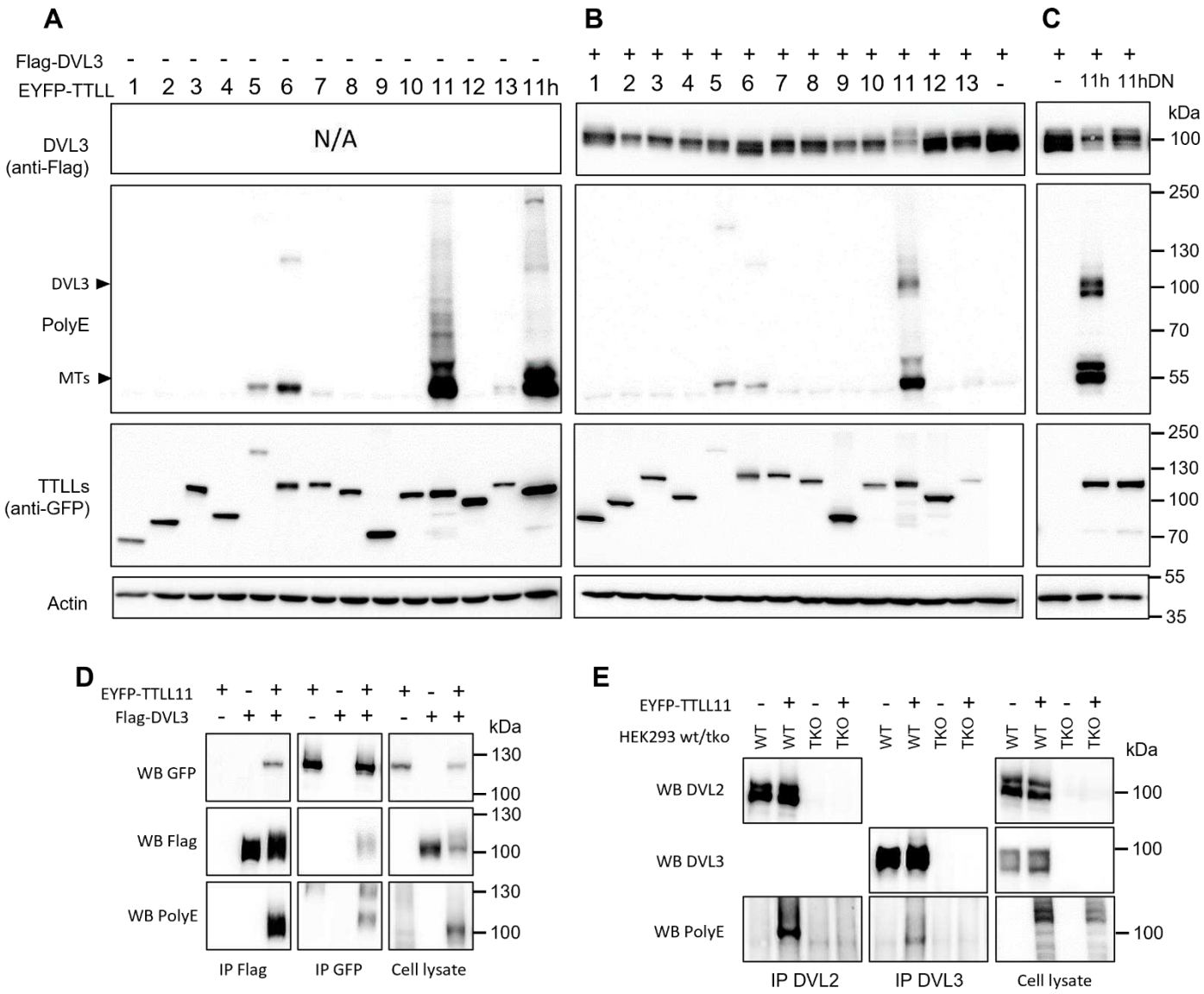

Fig. 1. TTLL11 binds and polyglutamylates DVL3. (**A**-**C**) HEK293T cells were transfected with constructs encoding murine EYFP tagged TTLL1 – TTLL13 together with control plasmid (A) or DVL3 (B), or DVL3 with human TTLL11 and its inactive variant TTLL11 (E531G; DN) (C). The samples were subjected to WB analysis using polyglutamylation specific antibody – PolyE. Note the appearance of polyE-positive bands of DVL3 size in conditions where TTLL11 and DVL3 were co-expressed. The corresponding experiment with DVL2 is shown in Fig. S1A and S1B. (**D**) Co-immunoprecipitation (co-IP) of Flag-DVL3 and TTLL11 overexpressed in HEK293T cells. TTLL11 is co-immunoprecipitated with DVL3; DVL3 in the pulldown was polyglutamylated when co-expressed with TTLL11 (IP Flag, WB PolyE). (**E**) IP of endogenous DVL3 and DVL2 from HEK293T cells in presence or absence of overexpressed TTLL11. Both endogenous DVL2 and DVL3 were polyglutamylated (WB PolyE). *DVL1/DVL2/DVL3* triple knockout (TKO) HEK293T cells served as a negative control. Abbreviations: Western blot (WB), immunoprecipitation (IP), microtubules (MTs), wild type (WT).

Fig. 2

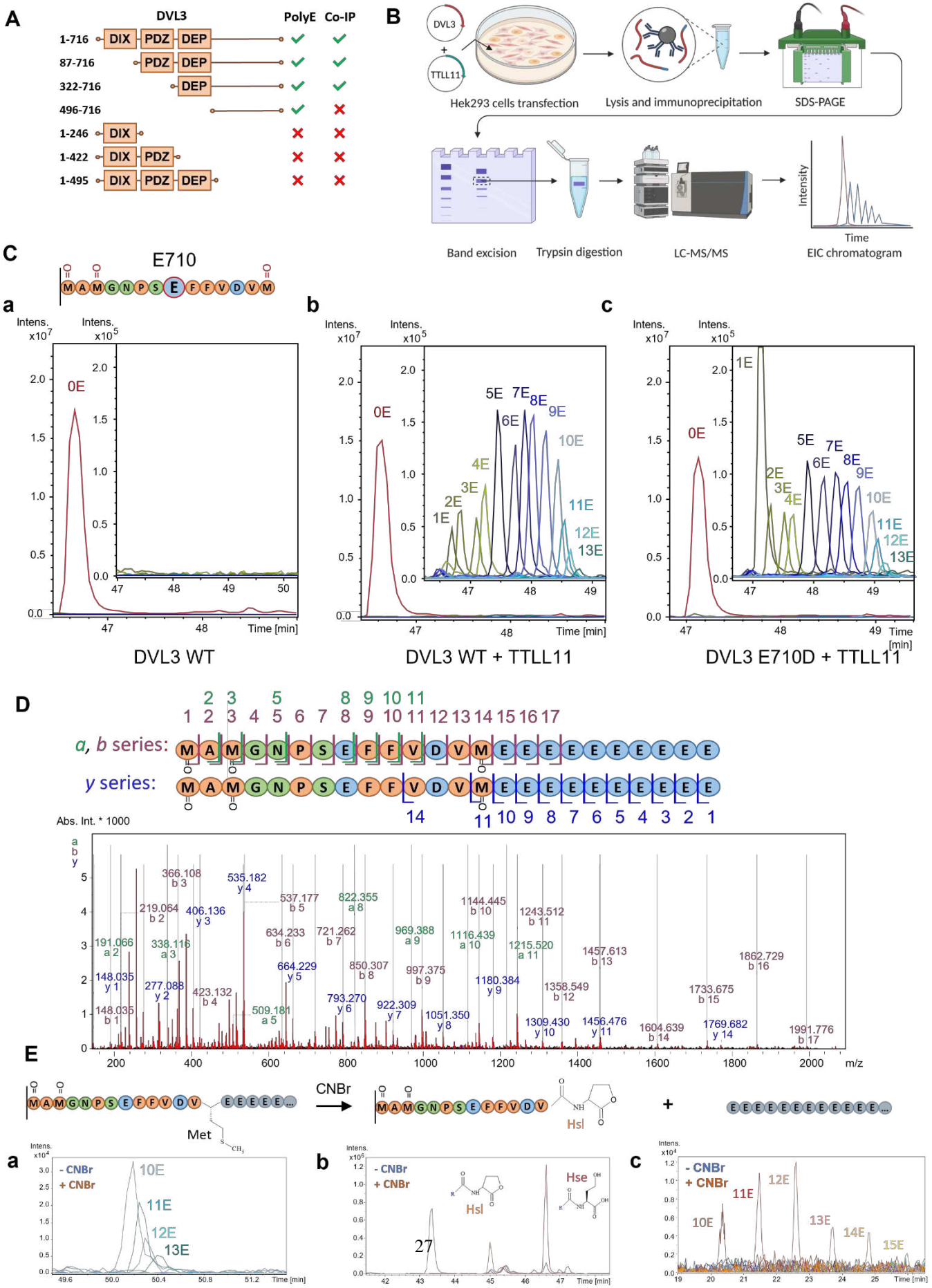

Fig. 2. Modification site of DVL3 polyglutamylation and a novel character of the PTM. (**A**) Domain mapping of DVL3 polyglutamylation. DVL3 truncation mutants were co-expressed with TTLL11 in HEK293T, DVL3 was immunoprecipitated and interaction with TTLL11 and DVL3 polyglutamylation was detected by anti-GFP and PolyE antibody, respectively. Raw data are shown in **Fig. S2A.** (**B**) Scheme of the sample preparation for mass-spectrometry (MS)-based analysis of polyglutamylation. (**C**) MS analysis of DVL3 polyglutamylation. The C-terminal tryptic peptide of DVL3 (schematized) was found to be polyglutamylated by TTLL11. EIC chromatogram shows peaks of this peptide in DVL3 (**a**), DVL3 co-expressed with TTLL11 (**b**) and DVL3 E710D in presence of TTLL11 (**c**). Polyglutamylated variants (blue lines) which are zoomed in a separate window. Only peaks corresponding to 3x M-ox peptide are shown, all peaks for 0 – 3x M-ox C-terminal peptides are shown in **Fig. S2 C, D**. (**D**) MS/MS fragmentation analysis of polyglutamylated DVL3 C-terminal peptide (3x M-ox variant). The peaks in a, b and y series observed are highlighted by green, purple, and blue color respectively. MS/MS spectra of control synthetic peptides with 10E modification at M716 or E710 in comparison to the polyglutamylated DVL3 immunoprecipitated from cells is shown in **Fig. S3**. The aa sequences for individual fragments are shown in schematic representation above the chromatogram. (**Ea-c**) Confirmation of C-terminal modification by CNBr cleavage. EIC shows peaks corresponding to polyglutamylated DVL3 C-terminal peptide before (blue) or after CNBr treatment (orange). C-terminal homoserine (Hse), homoserine lactone (Hsl) and free glutamate chains (10E-15E) are detected only after CNBr treatment. Hse or Hsl with polyE chain were not detected. The data shown correspond to 2x M-ox peptide; other M-ox variants are shown in **Fig. S4A-D**. Scheme (B) was created with BioRender.com.

1179

Fig. 3

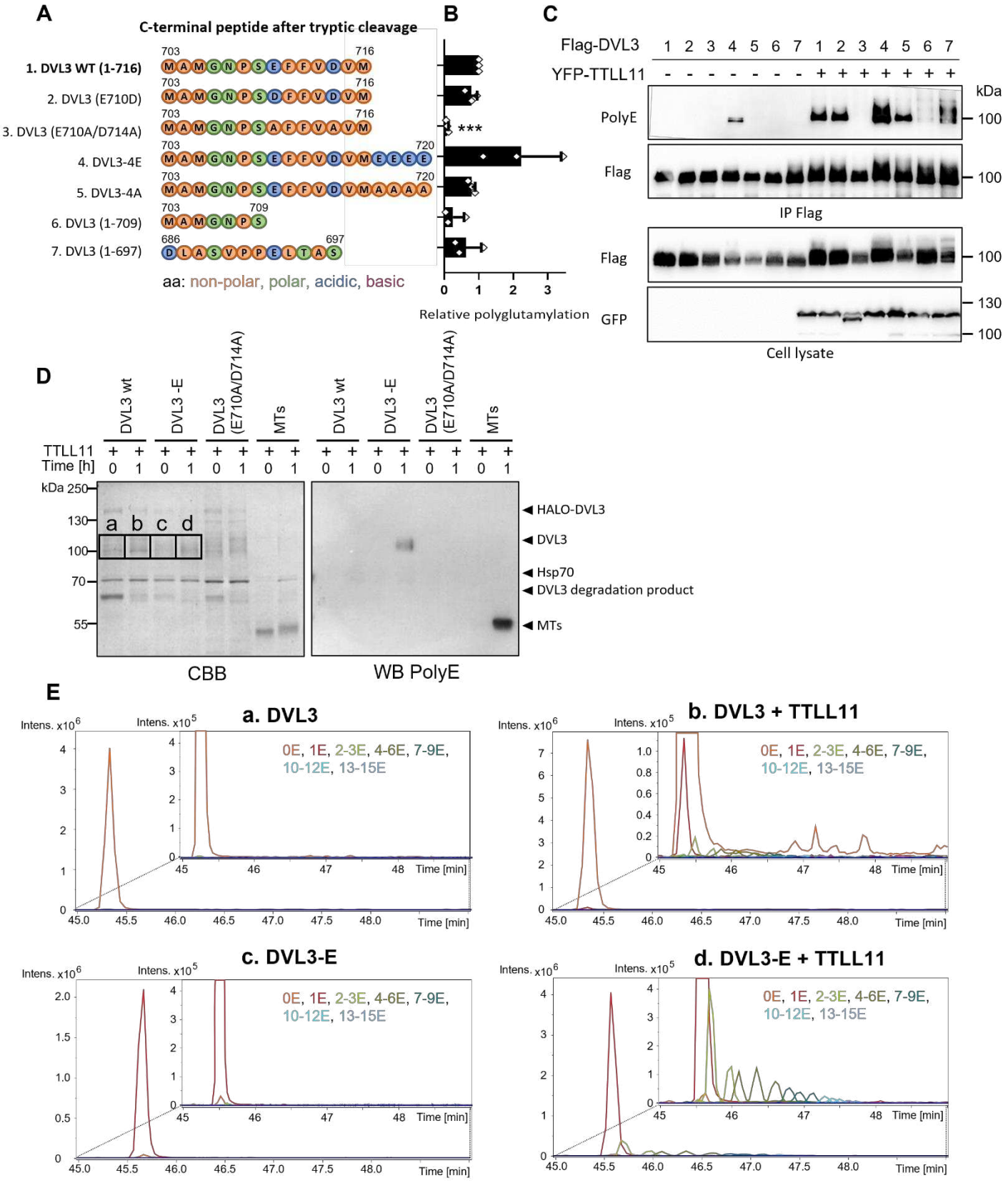

Fig. 3. Sequence determinants of TTLL11-mediated DVL3-polyglutamylation. (**A**) Schematic representation of DVL3 mutants. (**B**, **C**) HEK293 cells were transfected with the indicated Flag-DVL3 mutants and EYFP-TTLL11. DVL3 variants were immunoprecipitated and the extent of polyglutamylation was analyzed by anti-PolyE antibody (n=3). Relative polyglutamylation is represented as PolyE band intensity, normalized to total protein (Flag) signal, and shown as a fold change compared to Dvl3 WT polyglutamylation. Statistical significance was assessed using one-sample t-test with theoretical median = 1. (**D**, **E**) In-vitro polyglutamylation of purified DVL3/DVL3-E by TTLL11. The level of polyglutamylation was analyzed by SDS-PAGE followed either by Western blotting analysis using polyE antibody (D) or bands corresponding to DVL3 (indicated as **a-d** on Coomassie brilliant blue (CBB) stained gel) were excised and used for subsequent MS analysis. (E) EIC showing detection of in-vitro polyglutamylated DVL3 C-terminal peptide in the individual conditions (a-d).

Fig. 4

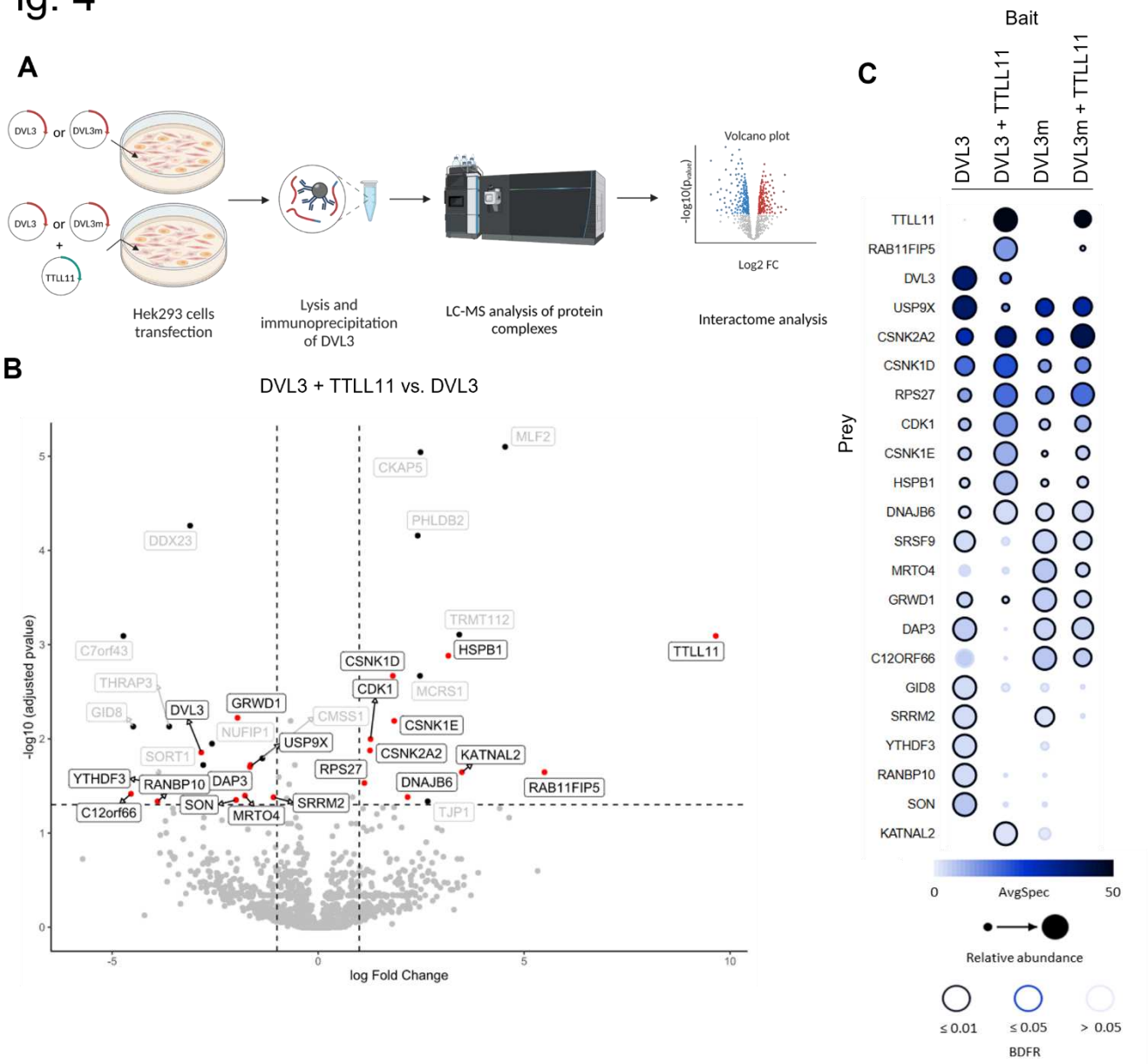

Fig. 4. Change of DVL3 interacting partners upon its polyglutamylation. (**A**) Scheme of sample preparation for MS analysis of DVL3 interactome upon co-expression with TTLL11. DVL3m = glytamylation defective DVL3 E710A/D714A. (**B**) Change of DVL3 interacting partners when overexpressed with TTLL11 was compared to overexpression of sole DVL3. DVL3 was immunopurified and interacting partners were analyzed by LC-MS. Volcano plot shows detection of significantly upregulated and downregulated interacting partners using LIMMA statistical test (FC $\geq$ 1, adjusted p value $<$ 0.05). Hits from LIMMA were further analyzed by REPRINT with integrated CRAPOME and SAINTexpress tools (**C**). The significantly changed proteins are highlighted in black in the Volcano plot (B). The scheme (A) was created with BioRender.com.

Fig. 5

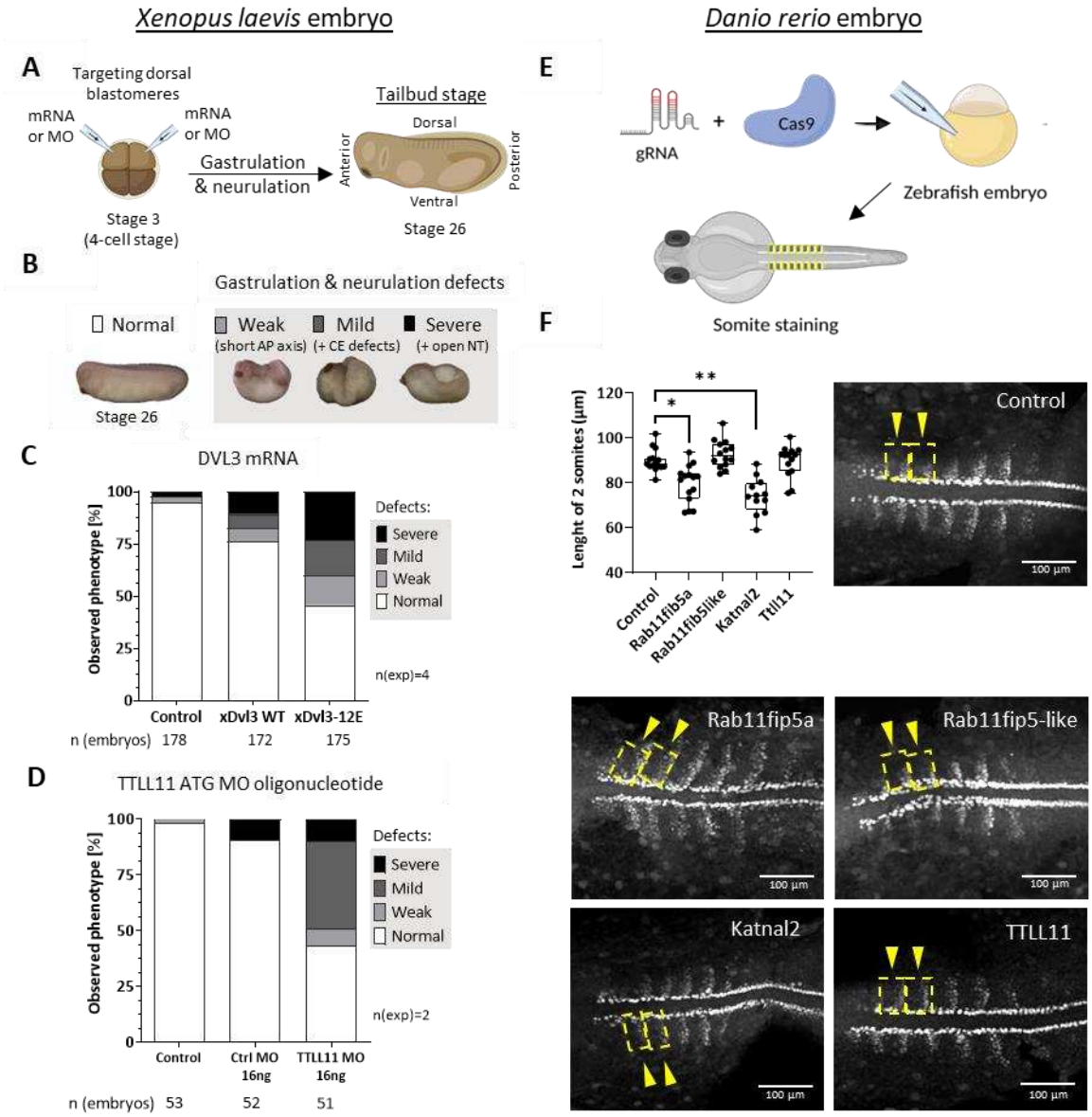

Figure 5. Role of DVL3 polyglutamylation in *Xenopus laevis* and *Danio rerio* embryonal development. (**A**) Both dorsal blastomeres of 4-cell *Xenopus laevis* embryo were injected with xDvl3 mRNA or xTTLL11 morpholino (MO) and embryos were observed during gastrulation and neurulation at stage 26. (**B**) Phenotypes in *Xenopus* gastrulation and neurulation were assigned to 4 groups: no defects and weak (short AP axis), mild (+ convergent extension defects), and severe defects (+ open neural tube). (**C**) Effect of xDvl3 WT and xDvl3-12E modification mimicking mutant mRNA injection. (**D**) Effect of MO targeting xTTLL11 ATG start codon injection (for splicing MO see Fig. S5G). (**E**) *Danio rerio* embryo was injected with Cas9 and gRNA targeting gene of interest. Embryos were fixed at 14.5 hpf and stained by α-MyoD1 antibody for somite visualization. (**F**) The length of the first 2 anterior somites was measured for control embryo and *Rab11fip5a*, *Rab11fip5-like*, *Katnal2*, and *TTLL11* KO embryos (n>12). Statistical analysis was performed by unpaired t test. Schemes in A and E were created with BioRender.com.

Fig. 6

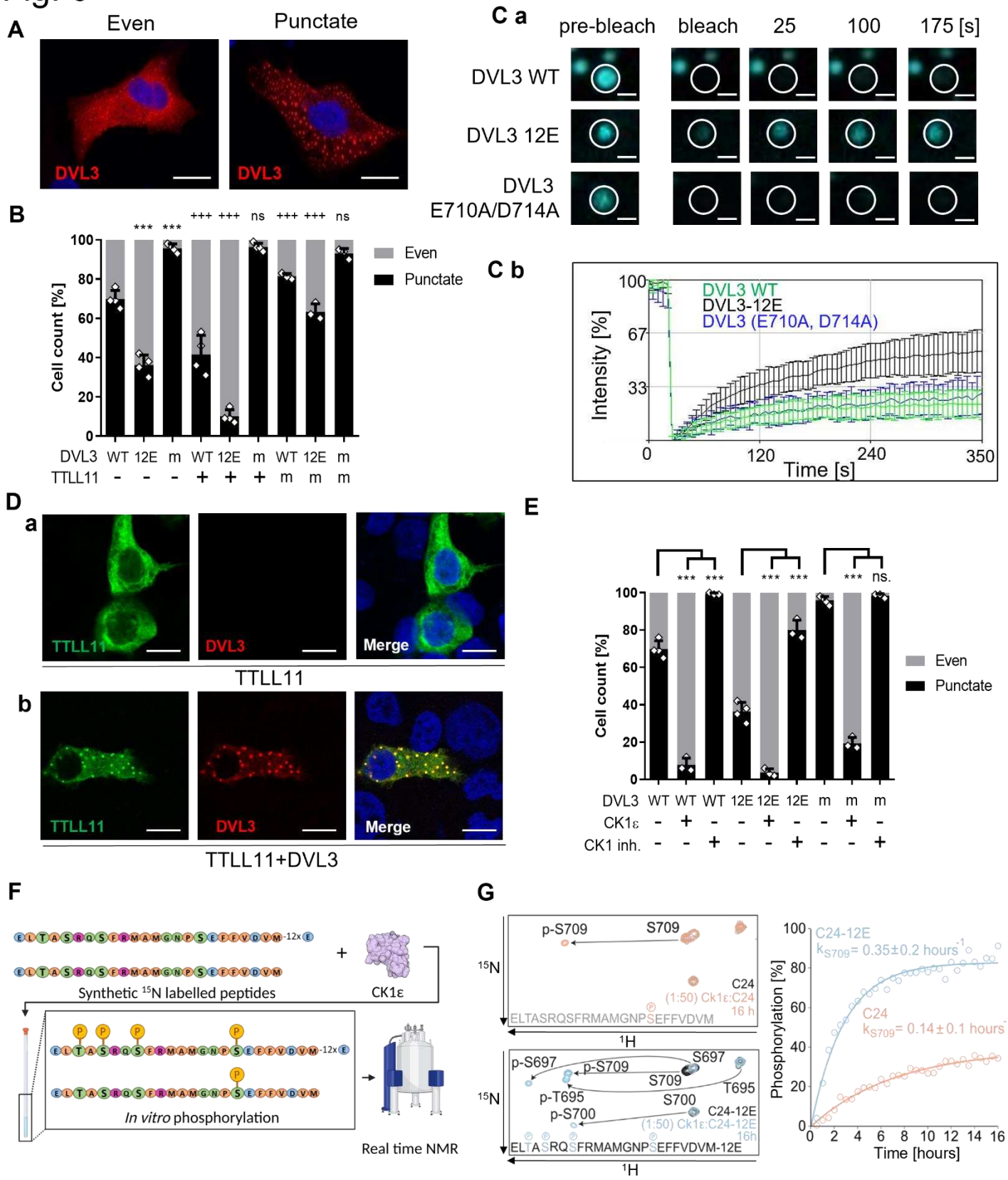

Fig. 6. Polyglutamylation of DVL3 alters its LLPS and promotes phosphorylation by Ck1ε. (**A**) Overexpressed DVL3 in HEK293T cells. Scale bar = 10 µm (**B**) Analysis of overexpressed DVL3 subcellular localization with its polyglutamylation variants in DVL1/DVL2/DVL3 triple KO HEK293 cells. Phenotype was assessed for >200 cells; N ≥ 3. Cell counts and SD are indicated. Statistically significant difference from WT DVL3 (*), or from the same DVL3 variant in the absence of TTLL11 or inactive TTLL11m (E531G) (+) is indicated. DVL3m = DVL3 E710A/D714A (**Ca**) FRAP analysis of ECFP-DVL3 WT, ECFP-DVL3-12E and ECFP-DVL3 E710A/D714A intracellular condensates. (**Cb**) Intensities of fluorescence summarized in the graph. The data represent average from 15 condensates in 3 biological replicates (5 droplets/replicate). Scale bar = 2 µm. Raw data are shown in **Fig. S7C**. (**Da**) Overexpressed TTLL11 in the absence or presence (**Db**) of co-expressed DVL3 in HEK293T cells. Scale bar = 10 µm. (**E**) Analysis of subcellular localization of DVL3 variants upon co-expression or inhibition of CK1ε by 1µM PF670462. Statistically significant differences from the condition without CK1ε/CK1 inhibitor is indicated for each DVL3 variant (*). Experiments from 6B, 6E and 7C were performed simultaneously, and control conditions are identical. ***/+++ represent $p < 0.001$; ns - not significant. (**F**) CK1ε *in vitro* phosphorylation of 24 DVL3 WT C-terminal aa (C24) or extended by 12E (C24-12E) peptides analyzed by NMR. Scheme was created with BioRender.com. (**G, left**) Overlay of HSQC spectra obtained before (grey and black for peptide C24 and C24-12E, respectively) and at the end of 16h reaction (orange and blue for C24 and C24-12E, respectively). Arrows indicate chemical shift caused by phosphorylation. (**G, right**) Time course phosphorylation of C24 (orange) and C24-12E (blue) peptides at S709. The apparent rate constants were estimated from fitting to a single exponential function.

Fig. 7

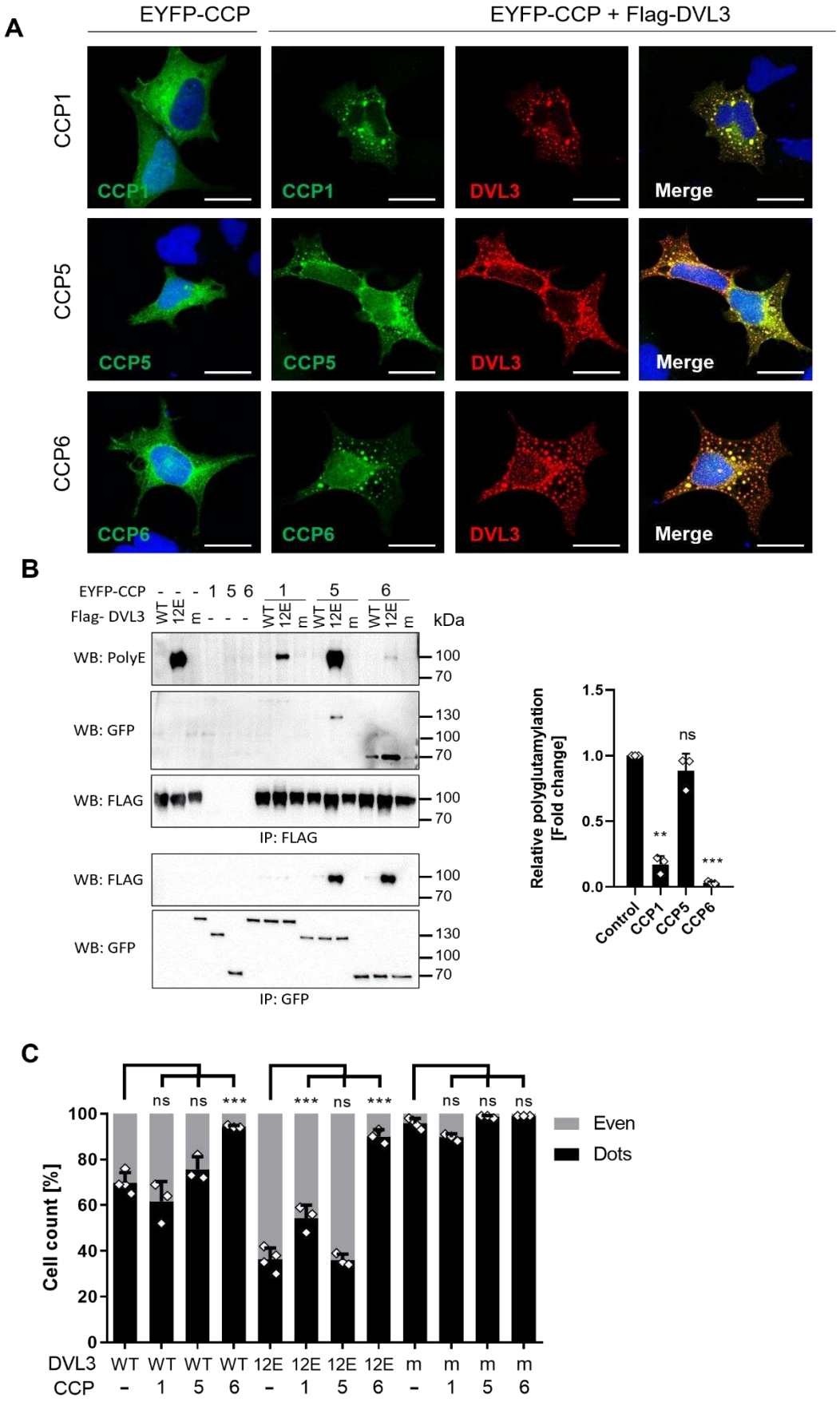

Fig. 7. Deglutamylation of DVL3 by CCP enzymes. (**A**) Co-localization of overexpressed DVL3 with EYFP tagged CCP1, CCP5 and CCP6 in RPE cells. CCPs are recruited from microtubule/even distribution into DVL3 puncta. DVL3 is visualized using primary anti-Flag and corresponding secondary Alexa Fluor 568 antibodies. Scale bar = 20 µm. (**B**) Deglutamylation and interaction of DVL3 by/with CCPs. DVL3 variants (DVL3 m stands for E710A/D714A mutant) were co-expressed with EYFP-tagged CCP1, CCP5 and CCP6 in HEK293T cells, lysed, immunoprecipitated using anti-FLAG antibody (DVL3) and anti-GFP (CCPs) and analyzed by Western blotting (WB). Polyglutamylation was detected by modification-specific antibody PolyE, quantified using ImageJ software and normalized on immunoprecipitated DVL3 protein amount (Flag antibody) in 3 independent replicates. Statistics were calculated by a one-sample t-test with theoretical mean=1. (**C**) Cells were transfected as in (B) but in DVL1/DVL2/DVL3 TKO HEK293T cells and subcellular localization of DVL3 was analyzed by immunocytochemistry. Subcellular localization of DVL3 was assessed for at least 200 cells in 3 independent replicates. Mean + SD is shown. Statistical significance in comparison to the condition without CCP for each DVL3 variant is shown. ** represents $p < 0.01$; *** represents $p < 0.001$, ns – not significant. Experiments from Fig 6B, 6E and 7C were performed simultaneously, and control conditions are identical.